Cholinergic and noradrenergic axonal activity is both strongly coordinated with behavioral state and heterogeneous across the dorsal cortex

Lindsay Collins[1], John Francis[1], Brett Emanuel[1], and David McCormick[1,2]

[1]Institute of Neuroscience, University of Oregon, Eugene, OR, USA, 97405

[2]**Corresponding author**: David McCormick (davidmc@uoregon.edu)

The authors declare no conflicts of interest.

This work was funded by National Institutes of Health (NIH) R35NS097287 and R01NS118461. We would like to acknowledge the members of the McCormick lab for helpful discussions while preparing this manuscript.

Abstract

Fluctuations in brain and behavioral state are supported by broadly projecting neuromodulatory systems. In this study, we use mesoscale two-photon calcium imaging to examine spontaneous activity of cholinergic and noradrenergic axons in awake mice, in order to determine the interaction between arousal/movement state transitions and neuromodulatory activity across the dorsal cortex at distances separated by up to 4 mm. We confirm that GCaMP6s activity within axonal projections of both basal forebrain cholinergic and locus coeruleus noradrenergic neurons track arousal, indexed as pupil diameter, and changes in behavioral engagement, as reflected by bouts of whisker movement and/or locomotion. The broad coordination in activity between even distant axonal segments indicates that both of these systems can operate in a global fashion, especially in relation to changes in behavioral state. In addition to this broadly coordinated activity, we also find that a subpopulation of both cholinergic and noradrenergic axons exhibit heterogeneity in activity that appears to be independent of our measures of behavioral state. By monitoring the activity of cholinergic interneurons in the cortex we found that a subpopulation of these cells exhibit state-dependent (arousal/movement) activity. These results demonstrate that cholinergic and noradrenergic systems not only provide a prominent and broadly synchronized signal related to behavioral state, but may also provide more heterogeneous activity independent of this general signal. Together, these two systems may prepare the cortex for both broad behavioral state transitions as well as regionally or temporally specific cortical dynamics.

Introduction

Rapid, moment to moment fluctuations in arousal state occur across species, from mice to humans, and have a significant impact on both cortical (and subcortical) activity and the ability to perform behavioral tasks (reviewed in McCormick, Nestvogel, and He 2020; Flavell et al. 2022; Lee and Dan 2012). In mice, rapid behavioral state fluctuations are coupled with broad changes in cortical excitation and are often accompanied by changes in arousal (pupil diameter), or movement (locomotion or orofacial movement; (Salkoff et al. 2020; McGinley, David, and McCormick 2015; McGinley et al. 2015; Musall et al. 2019; Stringer et al. 2019).

The neuromodulators acetylcholine (ACh) and noradrenaline (NA) are believed to contribute to these cortex-wide fluctuations in neural dynamics by sending signals via broadly projecting axonal pathways (Kim et al. 2016; Schwarz and Luo 2015; Mobley and Greengard 1985; Chandler and Waterhouse 2012; Mechawar, Cozzari, and Descarries 2000). The release of either ACh or NA can significantly impact the activity of single cortical neurons and how these neurons interact in local and long range networks. For example, ACh can depolarize cortical neurons by binding to both metabotropic muscarinic and ionotropic nicotinic receptors, thereby reducing slow oscillations and facilitating higher-frequency rhythms, hallmarks of increased arousal (Metherate, Cox, and Ashe 1992; Hedrick and Waters 2015; Dasgupta, Seibt, and Beierlein 2018). Similarly, NA suppresses slow oscillatory activity in the cortex via metabotropic receptors (Sara and Bouret 2012). Activity patterns of cholinergic and noradrenergic neurons are highly correlated with arousal and behavioral state fluctuations. For example, cortical ACh activity increases during bouts of active whisking (Eggermann et al. 2014) as well as during running and licking (Harrison et al. 2016; Reimer et al. 2016), and optogenetic activation of either NA neurons in the locus coeruleus (LC) or ACh neurons in the basal forebrain (BF) promotes wakefulness and locomotor activity (Carter et al. 2010; Irmak and de Lecea 2014). Moreover, both cortical ACh and NA activity in primary auditory and visual cortices track pupil dilation/constriction (Reimer et al. 2016; Nelson and Mooney 2016b; Larsen and Waters 2018). Such studies provide clear evidence that both ACh and NA are involved in the modulation of arousal state and cortical neuronal/network dynamics.

In addition to the broad arousal-based neuromodulation described above, anatomical and functional evidence suggests that cholinergic and noradrenergic systems also provide more regionally specific signaling. The basal forebrain-derived cholinergic (BF-ACh) system is topographically organized such that sub-regions within the BF preferentially project to different cortical and subcortical targets (Huppé-Gourgues, Jegouic, and Vaucher 2018; Zaborszky et al. 2015; Gielow and Zaborszky 2017), and activation of distinct regions of the BF results in desynchronization of restricted cortical regions (Kim et al. 2016). Recent recordings from cholinergic neurons in different regions of the BF reveal a common signal strongly related to behavioral state, but also some degree of heterogeneity (Robert et al. 2021). In addition to BF-derived cholinergic signaling, the cortex also receives input from local cortical VIP-expressing interneurons (VCINs) that release ACh, GABA, or both, depending on their specific presynaptic release machinery (Granger et al. 2020). While many superficial layer VIP interneurons exhibit activity related to arousal/movement (Fu et al. 2014; Yu et al. 2019; Petersen 2019; Muñoz et al. 2017; Reimer et al. 2014; Dipoppa et al. 2018; Poulet and Crochet 2018), it is unclear how

homogeneous or heterogeneous the activity of cholinergic VCINs is in association with arousal or behavioral (e.g. movement) state.

Within the locus coeruleus-derived noradrenergic (LC-NA) system, synchronized activity between LC neurons is often observed in relation to increases in behavioral engagement/vigilance to external events or stimuli (reviewed in Aston-Jones and Cohen 2005; Poe et al. 2020; Sara 2009), while modularity is strongly suggested by evidence of topographically distinct projection patterns (Loughlin, Foote, and Bloom 1986; Loughlin, Foote, and Fallon 1982; Waterhouse et al. 1983; Chandler, Gao, and Waterhouse 2014)) and paired recordings in the rat LC which can show little synchrony in spontaneous or evoked activity, at least under conditions of anesthesia (Totah et al. 2018; Noei et al. 2022). Recent investigations in awake, behaving mice reveal some level of heterogeneity in neuronal activity between different LC neurons in relation to behaviorally relevant components on learned and rewarded tasks (Breton-Provencher et al. 2022; Uematsu et al. 2017).

Together, evidence suggests that a broadly synchronized, arousal and/or behavioral state-dependent component of cholinergic and noradrenergic activity may operate alongside a more local, task-specific component. Here, through simultaneous imaging of GCaMP6s expressed in multiple ACh or NA axons (and local cholinergic interneurons) across the dorsal cortex, we present evidence for both broad cholinergic and noradrenergic state-dependent signaling as well as more heterogeneous activity during spontaneous behaviors in the waking state.

Results

Relationship between neuromodulatory activity and behavioral state

To investigate the relationship between cholinergic (ACh) and noradrenergic (NA) dorsal cortical axon activity and behavioral state, we used 2-photon mesoscope imaging to record GCaMP6s fluorescence in BF (basal forebrain)-ACh and LC (locus coeruleus)-NA axons in the cortex while recording facial movements, pupil diameter, and locomotion on a running wheel (Fig. 1A) in awake, head-fixed and habituated mice. To image BF-ACh axons, injections of an axon-targeted GCaMP6s calcium sensor were made into the BF (N = 5 mice, n = 397 axon segments; see Methods). To image NA axons originating from the LC (Giustino and Maren 2018), a cre-dependent, transgenically encoded GCaMP6s calcium reporter line was crossed with a DBH-cre line (N = 6 mice, n = 283 axon segments; see Methods).

To achieve a wide range of behavioral states, we habituated mice to the experimental set-up over 1-3 sessions such that the state of the animal varied from quiet resting in which movement was limited to occasional whisker twitches (this state is typically associated with smaller to medium sized pupil diameters), to frequent, but non-continuous, movements of the whiskers/face (typically associated with moderately large pupil diameters), to prolonged (seconds) bouts of walking/running (typically associated with large pupil diameters; (McGinley, David, and McCormick 2015; Reimer et al. 2014). Our habituated mice typically spent the majority of their time awake (see Methods), but not walking. This resting state was

characterized by frequent, but brief (< 0.5 second) bouts of whisker “twitches” (see movie S1), presenting as sudden movements of the whisker pad interspersed with periods without movement (Fig. 1D, F). In addition to whisker twitching, mice also often exhibited > 1 sec bouts of “whisking” characterized by large forward-backward swings of the whiskers (see movie S1, S2) with or without walking/running. Both whisker twitches and whisking were associated with movements of other portions of the face (e.g. snout, jaw) and increases in pupil diameter (see Fig. 3 below). Interspersed within these periods of non-walking, the mouse occasionally would walk or run on the circular wheel for 2 s or more. These bouts of locomotion were accompanied by forward-backward movements of the whiskers, occasional eye movements (especially at the beginning of walking), and significant increases in pupil diameter (Fig. 1D, F).

To image cholinergic or noradrenergic axon segments during variations in behavioral state, regions of interest (ROIs) were selected from across the dorsal surface of the neocortex at an imaging depth from the surface of the brain of approximately 100 - 200 µm (putative deep layer 1 and superficial layer 2/3). Simultaneous recordings were obtained from ROIs separated by up to approximately 3.5 mm for the BF-ACh axons and 4 mm for the LC-NA axons (Fig. 1B). Selected axon segments were chosen from putative retrosplenial, somatosensory, primary and secondary motor, and visual cortices (regions defined using coarse alignment to the Allen Brain Institute Common Coordinate Framework; Fig. 1B; Wang et al. 2020). Simultaneously imaged axon segments were always in the same hemisphere.

Examination of individual axon segment recordings, averages of axon segments recorded within the same region of interest (ROI; 50x50 to 400x400 µm), and averages of all axon segments simultaneously monitored revealed activity that closely tracked behavioral state (Fig. 1D-G), across all dorsal cortical regions monitored (Fig. 1B). Both cholinergic and noradrenergic axon GCaMP6s activity increased markedly in relation to whisker pad movement (twitching or whisking) and walking (Fig. 1D-G; Fig. S1; movie S2). A striking similarity was apparent between the patterns of activity in different axons, even if these axon segments were from distant recording locations. While both cholinergic and noradrenergic axons exhibited activity that was clearly related to behavioral state (as measured by whisker movements and walking), there was also an apparent difference between these two systems. GCaMP6s activity in the noradrenergic axon segments was more transient than in cholinergic axon segments during a prolonged walking bout (cf. Fig 1E, G; see also Fig. 2D,E below), consistent with previous reports (see also below; Reimer et al. 2016).

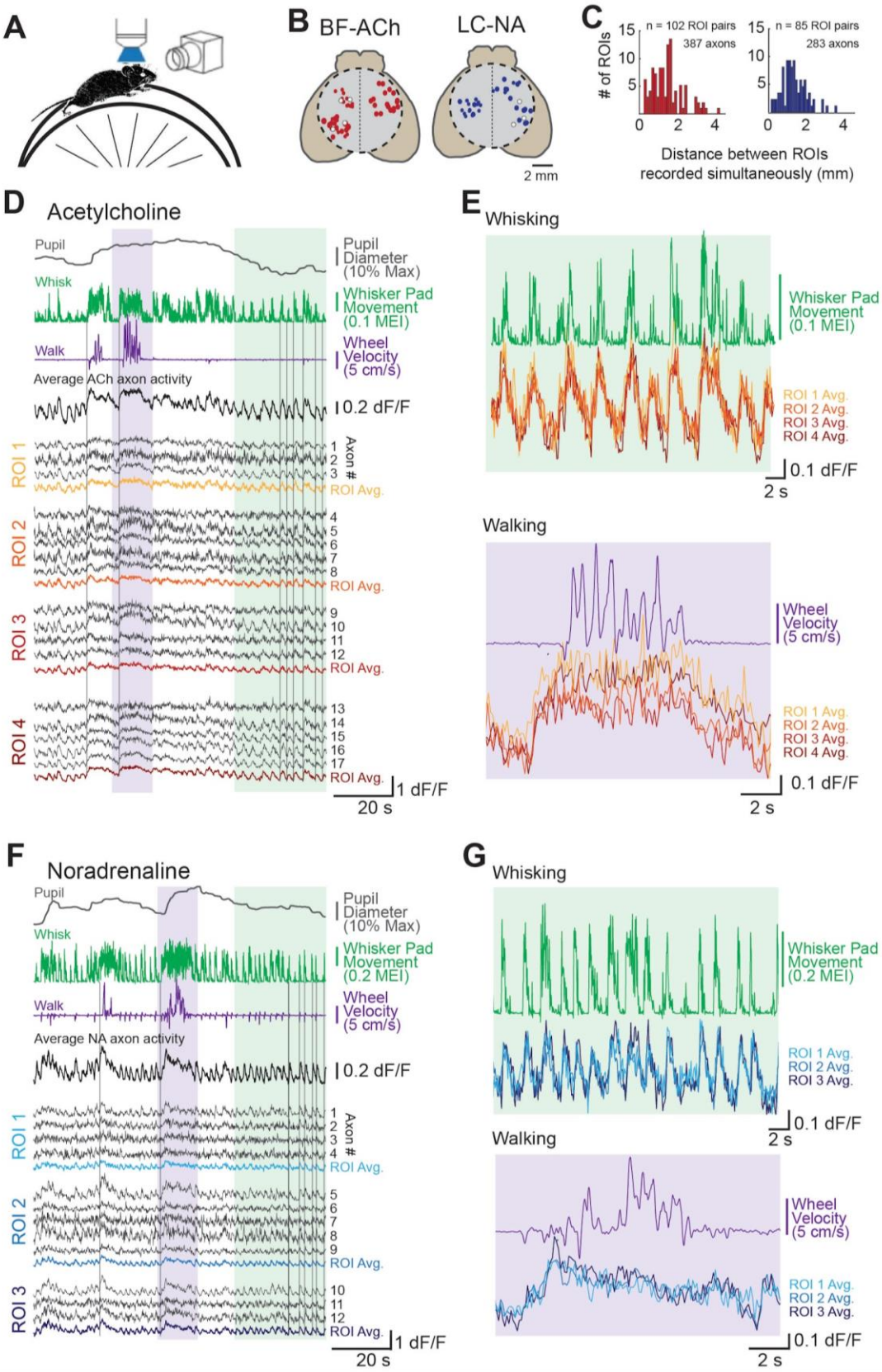
A
B BF-ACh
LC-NA
2 mm
C
n = 102 ROI pairs
387 axons
n = 85 ROI pairs
283 axons
# of ROIs
Distance between ROIs recorded simultaneously (mm)
D Acetylcholine
Pupil
Pupil Diameter (10% Max)
Whisk
Whisker Pad Movement (0.1 MEI)
Walk
Wheel Velocity (5 cm/s)
Average ACh axon activity
0.2 dF/F
ROI 1
ROI 2
ROI 3
ROI 4
Axon #
ROI Avg.
1 dF/F
20 s
E Whisking
Whisker Pad Movement (0.1 MEI)
ROI 1 Avg.
ROI 2 Avg.
ROI 3 Avg.
ROI 4 Avg.
0.1 dF/F
2 s
Walking
Wheel Velocity (5 cm/s)
F Noradrenaline
Pupil
Pupil Diameter (10% Max)
Whisk
Whisker Pad Movement (0.2 MEI)
Walk
Wheel Velocity (5 cm/s)
Average NA axon activity
0.2 dF/F
ROI 1
ROI 2
ROI 3
Axon #
ROI Avg.
1 dF/F
20 s
G Whisking
Whisker Pad Movement (0.2 MEI)
ROI 1 Avg.
ROI 2 Avg.
ROI 3 Avg.
0.1 dF/F
2 s
Walking
Wheel Velocity (5 cm/s)

Figure 1. 2-photon imaging of dorsal cortical cholinergic and noradrenergic activity reveal strong state dependence. A. Schematic of experimental setup. Awake mice were placed atop a running wheel underneath a 2-photon mesoscope objective for imaging of axonal activity through GCaMP6s. A second side camera was used to capture facial movements. **B.** To allow for imaging across a large region of cortex, mice were implanted with an 8 mm diameter glass cranial window (dotted circle) on the dorsal brain surface. Recordings could be collected from regions of interest (ROIs) within a 5x5 mm field of view. Estimated locations of all ROIs are shown for all BF-ACh (left) and LC-NA (right) axon segment recordings. Size of each circle corresponds to the size of the corresponding square ROI, ranging from 50x50 to 400x400 µm. Typically 3 or 4 ROIs, always within the same hemisphere, were used for imaging. White circles represent ROIs shown in panels D-G. **C.** Frequency histogram of the distance between simultaneously recorded ROIs during BF-ACh (left) and LC-NA (right) experiments. **D-G.** Example recordings of GCaMP6s activity in 17 BF-ACh simultaneously imaged axon segments in 4 ROIs (D,E) and 13 LC-NA axon segments in 3 ROIs LC-NA (F,G). Pupil diameter, whisker pad movement (represented as motion energy index, MEI, as described in Methods), and wheel movement (both rotational and vertical) are shown alongside dF/F of individual axons recorded simultaneously across ROIs shown in panel B. Vertical gray lines in D and F are for reference and are aligned to the onset of examples of walking or whisker movements (see Movies S1, S2). Average activity across all axons simultaneously monitored as well as within a ROI are shown (D,F). Colored regions in D and F are expanded for illustration in E and G. Axon GCaMP6s data in E and G are represented as ROI averages.

To examine the relationship between cholinergic and noradrenergic axon activity and behavioral state transition, we aligned axonal recordings to the onsets and offsets of facial whisker pad twitches, whisking bouts, and walking bouts (Fig. 2A-C, respectively; Fig. S1). We confirmed that any movement-related axonal responses were not affected by motion artifacts by comparing GCaMP6s fluorescence to non-activity-dependent autofluorescence in small blebs within the imaging field (Fig. 2A-C, blebs; see Methods). Whisker twitches were defined as whisker pad movements that lasted less than 0.5 s, while a whisking bout was defined as whisker pad movement that lasted longer than 1 s. Both were required to be preceded by a period of 1 sec of non-whisker movement to be included in our analysis. For BF-ACh recordings, 397 axon segments were imaged in 5 mice during 1108 twitches, 330 whisking onsets, 201 whisking offsets, and 101 walking bouts. For LC-NA recordings, 283 axon segments were imaged in 6 mice during 644 whisker twitches, 400 whisking onsets, 353 whisking offsets, and 34 walking bouts.

At the onset of both facial movements/twitches, as well as whisking bouts (which involve both larger and more prolonged movements of the whiskers than whisker twitches), both BF-ACh and LC-NA axonal activity sharply increased (Figs. 2A, B; S1). Expanding the time base revealed that the onset of these increases in average BF-ACh and LC-NA axonal activity occurred, on average, nearly simultaneously with the onset of whisking (Fig. 2B, insets). Whisker movements reached their peak prior to GCaMP6s fluorescence (Fig. 2B, insets), presumably owing, at least in part, to the slower kinetics of intracellular calcium dynamics and the GCaMP6s fluorescence reporter mechanism (Chen et al. 2013) in comparison to whisker movements (see Fig. S3). Both cholinergic and noradrenergic axon activity decreased along with whisker movement just prior to onset of whisker twitches or a bout of whisking (Fig. 2A,B). This decrease in whisker movement and ACh/NA activity is the result of our requirement of no whisker movements for at least 1 second prior to the bout, for the bout of whisker movement to be included in our analysis (see Methods).

At the cessation of facial movement, BF-ACh and LC-NA axon activity decreased slowly (over 1-2 seconds; Fig. 2B offsets), in comparison to the rapid rise at movement onset (Fig. 2B). Previous studies of cholinergic and noradrenergic axonal GCaMP activity revealed that cholinergic fibers exhibit more sustained responses than noradrenergic axons during a bout of walking (Reimer et al. 2016). By examining whisking bouts of different durations, from 1 second

to > 5 seconds, we also observed that cholinergic axonal GCaMP6s responses are significantly more sustained than the noradrenergic axonal responses (Fig. 2D,E). For example, during prolonged (> 5 sec) bouts of whisking, the NA axonal response typically exhibited a strong increase in GCaMP6s fluorescence at the beginning of the whisking bout, which decreased over the next 0.5 to 1.5 seconds to a steady value that was on average 11% of the peak value (activity at 2-3 sec compared to peak, $t = -15.14$, $p < 0.0001$; Fig. 2E). In contrast, cholinergic fibers exhibited a more sustained response, such that the activity 2-3 seconds into the prolonged whisking bout was 93% of the peak (activity at 2-3 sec compared to peak, $t = 0.91$, $p = 0.36$; Fig. 2D).

The GCaMP6s activity of both BF-ACh and LC-NA axons increased prior to the onset, and slowly decreased at the offset, of a walking bout (Fig. 2C). To determine the uniformity of this response across axons and behavioral events (e.g. Fig. S1), we calculated the probability that a given axon would respond at the onset of a behavioral event (twitch, whisk, or walk). We defined “responsive” as a significant increase in dF/F between 1 s prior to event onset and 1 s following event onset (Fig. S1G,H; Student’s t-test, alpha = 0.01), in comparison to a distribution obtained from shuffled data (Fig. S1I,J). We found that a large number of BF-ACh and LC-NA axons increased activity at the onset of twitching (BF-ACh: 44.2 +/- 30.9%; LC-NA: 47.3 +/- 28.4%) and whisking (BF-ACh: 78.8 +/- 23.5%; LC-NA: 67.3 +/- 30.9%) bouts. On average, each BF-ACh axon significantly increased activity on 43.5 +/- 15.7% of twitching and 75.8 +/- 25.0% of whisking bouts. Similarly, on average, each LC-NA axon segment significantly increased activity on 46.7 +/- 13.7% of twitching and 74.4 +/- 24.4% of whisking bouts. These results indicate that, on average, with each whisker twitch, approximately half of NA and ACh axons will show increased activity responses, while with the transition to full whisking ~75% of NA and ACh axons are activated. At the onset of whisking bouts, simultaneously recorded axons were varied in their response even for whisking bouts that exhibited very similar changes in average axonal dF/F (Fig. S1K-O).

Walking bouts, which are associated with strong increases in cholinergic and noradrenergic activity (e.g. Figs. 1,2C; S2C) were not associated with a significant difference 1 second after walk onset in comparison to 1 second prior to walk onset, owing to an increase in average cholinergic and noradrenergic axon activity prior to walk onset that was approximately mirrored by a decrease in activity following walk onset (see Figs. 2C, S1C).

We suspected that the variable timing of axonal GCaMP6s activity observed with the onset and offset of a walking bout (e.g. Fig. S1 C,F) could reflect a variability of timing in behavioral state changes (e.g. as indicated by whisker movements) preceding and following bouts of walking. To test this hypothesis, we compared the onset/offset of whisker pad movement and walking. We observed that whisker pad movement is consistently initiated, with a variable onset, 0.5-5 s prior to walking initiation and typically persists for approximately 1-3 s, with a variable offset, after the cessation of walking (Fig. S2A,B). Thus, the lack of strong correlation between onset/offset of walking with cholinergic and noradrenergic activity is likely the result of a variable timing of onset/offset of whisking/arousal in relationship to walking bouts, and the strong association between ACh and NA axonal activity and behavioral state (which is tightly linked to whisker movements; Fig. 1E,G).

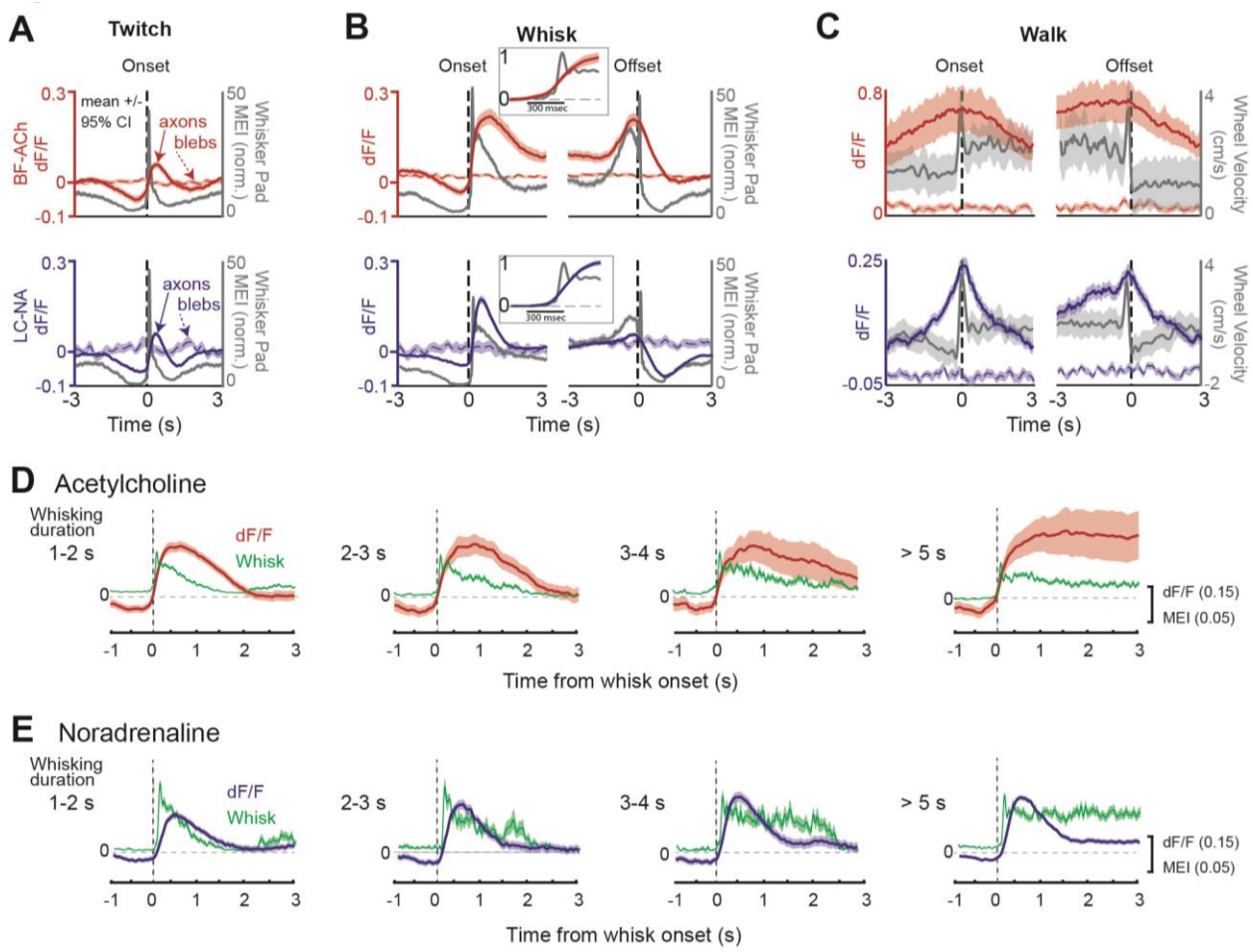

Figure 2. BF-ACh and LC-NA activity track behavioral state transitions. A-C. Mean GCaMP6s fluorescence in BF-ACh (top) and LC-NA (bottom) axons aligned to the onset and offset of whisker twitching (A), a bout of full whisking (B), and walking (C). Gray traces represent averaged whisker pad motion energy (A and B) or walking speed (C). Shaded region represents a 95% confidence interval. Fluorescence of nearby blebs (dotted lines) was not affected by whisking or walking. **B, insets.** Expanded time base, with data normalized from 0 to 1, for comparison of onset kinetics of average whisker movements and cholinergic/noradrenergic axon activity. **D, E.** Activation of cholinergic (D) and noradrenergic (E) axons during whisking bouts of varying durations, from 1-2, 2-3, 3-4, and > 5 seconds. Note that the cholinergic (red traces) axonal responses maintain activity during prolonged whisking (green traces), while the noradrenergic axonal responses (blue traces) are more transient. Shaded region represents a 95% confidence interval. For all panels, ACh data obtained from N = 5 mice, n = 397 axon segments over 1108 twitches, 330 whisking onsets, 201 whisking offsets, and 101 walking bouts. NA data obtained from N = 6 mice, n = 283 axon segments over 644 twitches, 400 whisking onsets, 353 whisking offsets, and 34 walking bouts.

Since we observed a strong relationship between whisker pad motion energy and modulatory axon activity, we wondered whether axon activity was linked to whisker movements per se, or to facial movement more generally. To answer this question, we compared the relationship between axon activity and motion of the whisker pad to the relationship between axon activity and motion of the mouth, snout, and full face in a subset of recordings comprising 65 BF-ACh axons and 50 LC-NA axons (Fig. 3A). Overall, these variables were highly correlated, as motion in one part of the face often accompanies motion in other regions of the face. However, we were able to identify occasional instances where facial motion was predominantly localized to the whisker pad, jaw, or snout regions (green, red, and yellow bars, respectively, in Fig. 3B) in all analyzed recording sessions.

First, we investigated the relationship between axonal activity and facial movements by calculating the coherence between GCaMP6s dF/F and movement within distinct regions of the face (jaw, snout, whisker pad) as well as movement across the full face. Previous studies have demonstrated a strong coherence at low frequencies (< 3 Hz) between cholinergic or noradrenergic cortical axonal activity and behavioral state, as measured by changes in pupil diameter (Reimer et al. 2016; Larsen and Waters 2018; Nelson and Mooney 2016a; Robert et al. 2021; Sturgill et al. 2020; Harrison et al. 2016) . In similarity to these studies, we found that coherence between both BF-ACh and LC-NA axon activity and facial movement was highest at low frequencies (< 1 Hz; Fig. 3C). Compared to walking speed and pupil dilation, we observed a stronger coherence between both BF-ACh and LC-NA axon activity and facial movements (including snout, jaw, whisker pad, and full face motion energy; Fig. 3C-D), suggesting that low frequency (< 1 Hz) facial movement is tightly coupled to changes in cholinergic and noradrenergic signaling in the cortex. The large drop in coherence between axonal activity and measures of behavioral state at frequencies above approximately 1 Hz likely represents more of a limitation of our imaging method to detect axonal activity at these frequencies, than a true lack of coherence (see Fig. 4A-E below and Methods; Fig. S3). Indeed, examining the distribution of power in our GCaMPs signal from cholinergic and noradrenergic axons reveals a strong drop off above approximately 1 Hz, such that very little power is observed at frequencies above approximately 2-4 Hz (Fig. S3). Thus, our study of comparing activity in cholinergic and noradrenergic axons across the cortex with behavioral state is most relevant to low frequency (< 1 Hz) events, similar to previous investigations (Reimer et al. 2014).

The temporal relationship between BF-ACh activity and facial movement, as measured by cross-correlation, was closely time-locked such that axonal activity was observed very shortly (within 100-200 ms) following the onset of facial movements (Fig. 3E). This delay is approximately the same as the rise-time required for GCaMP6s to bind Ca^{2+} and fluoresce in response to the initiation of action potentials (100-150 ms; Chen et al. 2013), indicating that the behavioral state-dependent onset of facial movements and increased activity in the BF-ACh system occurred within a relatively short time period, beyond our ability to resolve (see also Fig. 2B insets).

We determined the predictive power of each of the 6 behavioral arousal measures (pupil diameter, walking velocity, and motion energy of the whisker pad, snout, jaw, and full face) on axon activity using ridge regressions to avoid overestimation resulting from multicollinearity of predictor variables, since arousal state variables are not independent. The full model accounted for 33.3 +/- 2.9% of variance in BF-ACh axonal activity (Fig. 3F). Movement of the whisker pad area explained more of the variance in BF-ACh axonal activity than any other variable (whisker pad movement explained variance = 24.1 +/- 2.8%; $F = 89.2$, $p < 0.0001$; One-Way ANOVA). Walking speed explained less variance in axon activity than any other behavioral measure (R^2 = -0.05 +/- 0.02). Movements of the snout were also informative, as were motion energy in the full face video (Fig. 3F).

Similar to BF-ACh, activity of LC-NA axons lagged facial movements by 100-200 ms and facial (whisker, snout, full face) movements explained more variance in the noradrenergic axonal signal than walking speed or pupil diameter (Fig. 3G; $F = 17.16$, $p < 0.0001$). Although

we used ridge regressions to avoid overestimation, there still is the possibility that the regression overestimated the relationship between axon activity and behavior. We used the "session permutation" method, as described in (Harris, 2021), to address this concern. Briefly, this method determines the likelihood of a correlation arising from truly non-correlated data by comparing the prediction error obtained from regressions of matching (simultaneously recorded) sessions, to the distribution of prediction error for regressions of all permutations of unmatched sessions. For both BF-ACh and LC-NA data sets, prediction error for matched whisking and walking datasets was low in comparison to the distribution of unmatched sessions; therefore, we conclude that the relationships determined by linear regressions are valid (Fig. S4).

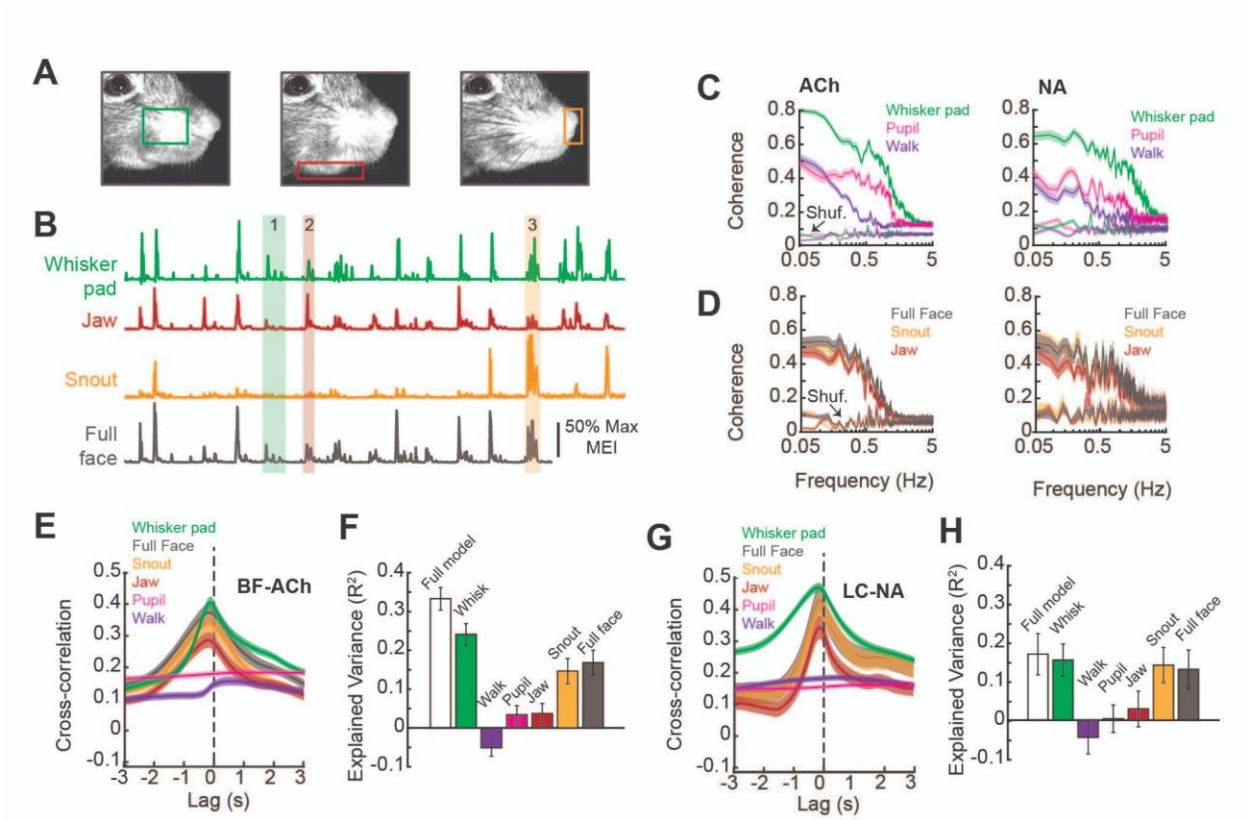

Figure 3. Facial movements are highly predictive of BF-ACh and LC-NA axon activity. A. Restricted regions within videos of the face were analyzed to capture movement of the (left to right) whisker pad, jaw, and snout. **B.** Example traces of the motion energy index (MEI) recorded from the whisker pad, jaw, snout, and across the entire frame (full face). Instances where motion energy of the face was predominated by whisker pad (1), jaw (2), or snout (3) movement are noted by green, red, and yellow bars, respectively. **C.** Coherence between average BF-ACh or LC-NA axon activity and movement of the whisker pad, walking, and pupil diameter. All simultaneously imaged axon segments within a session were averaged prior to calculation of coherence. **D.** Coherence between average BF-ACh or LC-NA axon activity and motion energy in the full face, snout, and jaw. It should be noted that examining coherence between adjacent segments of the same axon reveal our imaging method to be unable to accurately represent variations in activity above approximately 1 Hz, indicating a frequency limitation in the present coherence measures (see Fig. 4 and Fig. S3). **E.** Cross-correlation between arousal measures and BF-ACh axon activity. **F.** Amount of variance in BF-ACh axon activity that is explained by pupil, whisker movements, walking, snout movements, jaw movements, and movement energy in the full face view. **G-H.** Same as E-F for LC-NA axons. Error represents a 95% confidence interval for panels C-H. Results presented in E-H were obtained after low pass filtering signals at 1 Hz. For all panels, ACh data taken from N = 3 mice, n = 65 axon segments and NA data taken from N = 3 mice, n = 50 axon segments.

Evidence for Heterogeneity in Activity Between ACh and NA Axon Segments Across the Dorsal Cortex

To examine the possibility of both common and unique signals within cholinergic and noradrenergic axon segments across the cortex, we sought to measure the coherence and correlation in GCaMP6s signal between axon segments of the same modulatory system, as a function of distance and behavioral state (Fig. 4). Comparing the average coherence between all cholinergic/noradrenergic axon segments (excluding axon segments that were clearly portions of the same axons; see Methods) revealed a high level of average coherence at frequencies < approximately 1 Hz, and this group average coherence decreased markedly at frequencies above approximately 1 Hz (Fig. 4D,E, Exp. data). This high level of average coherence between simultaneously imaged cholinergic/noradrenergic axon segments at frequencies < 1 Hz suggests the presence of a strong common signal that is broadly expressed across these segments (Fig. 4D,E). The drop off in coherence at frequencies > 1 Hz is most likely a consequence of the frequency limitations of our data collection technique (see below and Fig. S3). While the average coherence between axon segments was high, there was a broad distribution of coherence between simultaneously monitored axon segments, as revealed by plotting the distribution of average coherence at frequencies between 0.05 and 0.5 Hz for all simultaneously recorded axon segments (Fig. 4D, E).

The broad range of relationships between activity in simultaneously recorded axon segments is also illustrated by examining the correlation of fluorescence between these segments (Fig. 4F,G). Comparison of axonal fluorescence correlations for both cholinergic (Fig. 4F) and noradrenergic (Fig. 4G) axons revealed a broad distribution, ranging from -0.03 to 0.99 for ACh and -0.09 to 0.93 for NA, with an average correlation of 0.54 +/- 0.19 for ACh and 0.51 +/- 0.16 for NA. The average correlations between ACh and NA axon segments decreased weakly with increased distance between segments (Fig. 4F,G), with the correlation between inter-axonal segment activity correlation and distance between segments being -0.12 ($p<0.001$) for ACh and -0.04 ($p = 0.05$) for NA. These results indicate that while cholinergic and noradrenergic axons are broadly correlated/coherent (at least at low frequencies) across the dorsal neocortex, they also exhibit a large degree of heterogeneity in these correlations/coherences.

Another way to visualize heterogeneity of activity between simultaneously monitored ACh and NA axonal segments is to compare their activity for overall average axonal responses that are of similar magnitude (see Fig. S1K-O). Even though the average response of the ACh of NA axons may be similar for two different bouts of whisker movement, the pattern of activity generated within the simultaneously monitored ACh or NA axon segments varied strongly. These variations gave rise to the strong appearance of whisker bout to whisker bout heterogeneity in axonal response patterns (see Fig. S1K-O).

To what degree are cholinergic and noradrenergic axons acting as if they are segments of the same axon?

To answer this question, we compared the results obtained in all axon segments with those obtained by comparing the activity in a random sample of sub-segments of the same axons (n=18 ACh axons; n=30 NA axons; Fig. 4). Comparing the average coherence between heterogeneous ACh and between heterogeneous NA axon segments with that obtained from

segments of the same ACh or NA axons revealed an overall lower average coherence in the heterogeneous population (Fig. 4D,E). Comparison of the distributions of coherence at frequencies of 0.05-0.5 Hz also revealed a broader distribution of coherence values for heterogeneous ACh and NA axon segments in comparison to segments of the same axons (Fig. 4D, E). Similarly, comparing the correlations between heterogeneous ACh and heterogeneous NA axons with segments of the same axons also revealed a significantly broader distribution in the heterogeneous sample (Fig. 4F, G). Comparing the signal-to-noise (SNR; see Methods) of the axon segments revealed that this heterogeneity in correlations for all axon segments versus segments of the same axon was not the result of higher SNR in the adjacent segments of the same axon in comparison to the general data set (Fig. S5C, D).

These results indicate that the heterogeneous axon segments are acting, as a population, in a manner that exhibits a larger variety of coherences and correlations than expected if the axon segments were all derived from the same axon.

Cholinergic and noradrenergic axons carry a common signal related to behavioral state

The presence of strong coherence and correlation between ACh or NA axon activity and behavioral state (e.g. whisker movements) suggests that coherence/correlations between axon segments may arise simply because they are both coherent/correlated to behavioral state. To examine the possibility of a common signal driving the correlation between axonal segments, we calculated a “common signal” as the average signal for all simultaneously imaged axon segments, minus the two axon segments under consideration (i.e. being correlated). This average or “common signal” is strongly coherent with movements of the whisker pad, especially at lower frequencies (Fig. 3C, D). Next, we calculated the partial correlation between these two axon segments, given the average of all other simultaneously imaged axon segments (i.e. the common signal, see Methods). Plotting the residual partial correlation versus the ordinary correlation revealed a large decrease for the vast majority of axon segments when this common signal is taken into account, such that the partial correlation centered around approximately 0 (ACh: 0.03 +/- 0.14; NA: 0.06 +/- 0.14; Fig. 4H, I). This result indicates that much of the ordinary correlation between axon segments, particularly at values below approximately 0.5-0.6, may have resulted simply from the correlation of the two axon segments to a common signal related to behavioral state.

At ordinary correlations above approximately 0.5-0.6 Hz, calculating the partial correlation by removing the common signal yielded a distribution whose mean was significantly above zero (Fig. 4H, I). Indeed, as the ordinary correlation approached 1, the partial correlation also approached this high value. One possibility is that these high ordinary and partial correlations may result from the monitoring of axon segments that were from the same cholinergic or noradrenergic axon. Another is that these axon segments are from different axons but nonetheless are highly correlated and generate activity that is independent of the common signal. We reasoned that comparing the ordinary and partial correlation of axon segments from the same axon may be instructive. If we were able to accurately capture all action potentials in two adjacent axon segments from the same axon, then both the ordinary and partial residual correlations should be 1 (e.g. see Fig. 5L for VCIN data), since action

potential activity in adjacent axon segments is expected to be identical (assuming no conduction failures; Foust et al. 2010; Popovic et al. 2011). If we were able to detect all action potentials, then taking into account a common signal, such as the average activity in other axons, would leave residual action potential activity in the adjacent axon segments that would still be identical - leading to a partial residual correlation of 1. However, our measure of activity is not action potentials, but GCaMP6s fluorescence, and the relationship of our measure of activity to true axonal action potentials is unknown. Revealing the distribution of data when comparing GCaMP6s signal between two adjacent axon segments of the same axon is instructive as to the limitations of our measures.

Comparing the partial correlation versus ordinary correlation between segments of the same cholinergic or noradrenergic axons revealed a striking increase in residual correlation (after taking the common signal into account) from near 0 to nearly 1, as the ordinary correlation increased from approximately 0.5 to 1 (Fig. 4H, I). The deviations away from a correlation of 1 between adjacent axon segments of the same axon, in both the ordinary and partial correlations, reveal a potential limitation in our ability to use GCaMP6s signaling to extrapolate the true activity relationship between axon segments. We hypothesize that our activity monitoring methodology results in a relatively weak and noisy GCaMP6s signal in fine cortical cholinergic and noradrenergic axons and that this noisy signal does not completely represent action potential-related changes in axonal $[Ca^{2+}]_i$, thereby resulting in correlations between adjacent segments of the same axon of less than 1. Another possibility is that adjacent axonal segments do indeed have significant variations in $[Ca^{2+}]_i$ levels with activity, and that even if action potential activity was identical between adjacent segments of the axon, variations in $[Ca^{2+}]_i$ were not. Our data cannot disentangle these two possibilities, since we do not have an independent measure of action potential activity and associated $[Ca^{2+}]_i$ fluctuations within these axon segments. Interestingly, when we performed the same analysis on two halves of the same VCIN cell bodies (which exhibit significantly stronger dF/F GCaMP6s signal, and have larger areas, than ACh and NA axons), we observed a correlation very near 1 for both ordinary and partial correlations (see Fig. 5 and below). We propose that the observed relationship between adjacent axon segments of the same axon is dictated by a simple rule: the larger the correlation in our measure of activity in adjacent axon segments when calculating ordinary correlation, the less likely removing the common signal will disrupt this correlation. This rule may account for the rise from near 0 to nearly 1 in partial correlation as the ordinary correlation increases from approximately 0.5 to 1 (Fig. 4H, I).

The distribution of data obtained from segments of the same axon overlapped strongly with data obtained from all axon segments (Fig. 4H,I). This result suggests that either the axon segments that were highly correlated are actually segments of the same axon (which is unknowable using our methodology) or that these axons are from different axons, but carry correlated activity that is independent from the common signall. We reasoned that if the high residual partial correlations were the result of the axon segments belonging to the same axon, then this partial correlation should decrease with distance, since the likelihood that the axon segments were from the same axon should also decrease with distance. Indeed, plotting the residual partial correlation for segments from the same axon versus other axons did reveal a significantly higher partial correlation for both cholinergic (same axon r = 0.40 +/- 0.31 vs

different axons r = 0.06 +/- 0.19; t = 8.41, p < 0.001) and noradrenergic (same axon r = 0.27 +/- 0.31 vs. different axons r = 0.01 +/- 0.28; t = 4.57, p < 0.001) axon segments (Fig. 4H,I inset). Comparing the change in partial correlation with distance revealed that for cholinergic axons, there is a significant (p<0.01) but small (r = -0.40) correlation between partial residual correlation and distance (Fig. 4J), while for noradrenergic axons, this decrease appeared to occur more rapidly with distance, dropping suddenly from 0.09 +/- 0.12 within the same ROI, to 0.04 +/- 0.10 between even the closest ROIs (< 1 mm away; t = -3.84, p < 0.001), and remaining 0.04 +/- 0.11 at further distances (Fig. 4J). The overall correlation between distance and residual partial correlation for NA axon segments was very low, but statistically significant (r = -0.15; p < 0.001). These low correlations with distance suggest that while our data may contain imaging from axon segments that are part of the same axon arbor in our heterogeneous population, this is not the main source of residual correlation following removal of the common signal.

What is the source of the common signal between axon segments? One possibility is that variations in behavioral state correlated with movement may represent a significant portion of the common signal. To test this hypothesis, we examined the degree to which taking the common signal (average axon segment activity) into account reduced the correlation between axons for different data sets: 1) full data set; 2) periods that exclude walking, but may include whisking; 3) periods that exclude both walking or whisking. To compare across axons with a wide range of correlation values, we subtracted the ordinary correlation from the partial correlation for each axon since higher ordinary correlations are associated with higher partial correlations. Compared to the partial correlation in the entire session, removing periods of walking did not have a significant effect. However, removing periods of both whisking and walking significantly (p < 0.01) lessened the difference between the partial and ordinary correlations (Fig. 4K). This result confirms that a significant portion of the common signal in ACh and NA axon activity results from behavioral state variations associated with whisker movements (see however, Fig. S5E,F).

Recently, it has been reported that cholinergic receptor activation across the dorsal cortex is decorrelated with increase in movement, suggesting that the cholinergic fibers projecting to different regions of the cortex may decorrelate with increased behavioral engagement (Lohani et al. 2021). However, our results indicate that the ability to make this conclusion may be severely affected by the limited ability to monitor noradrenergic/cholinergic activity using fluorescent reporting methods. Indeed, we observed a striking decrease in correlation between cholinergic (and noradrenergic) axon segments during walking (Fig. S5G,H). However, we obtained the same result when comparing adjacent axon segments from the same axon (which should remain highly correlated throughout all behavioral states), indicating that this movement-related decorrelation in fluorescence based activity is most likely an artifact of frequency-limited fluorescence-based data collection methods. Since we cannot resolve individual action potentials within axons at all frequencies, we are unable to measure whether there is, or is not, a decorrelation of activity between these axons during walking or whisking.

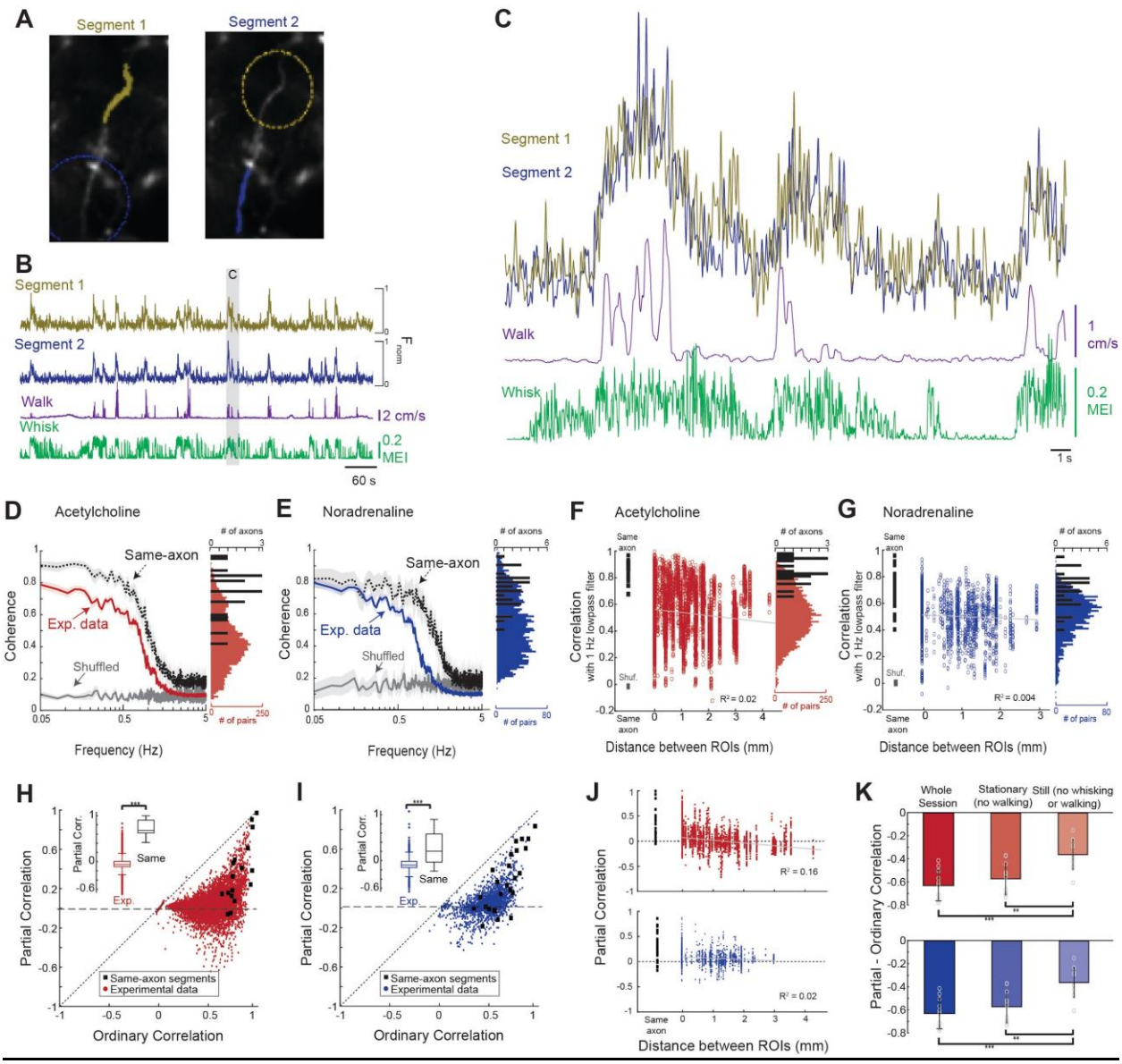

Figure 4. Cholinergic and noradrenergic axon segments across the dorsal cortex exhibit both a common signal related to behavioral state and signal heterogeneity. **A.** To examine the relationship between monitored axon segments, we first measured the relationship between GCaMP6s Ca^{2+} fluorescence signals measured in adjacent segments of the same axon (e.g. yellow labeled segment 1 vs. blue labeled segment 2; dotted circles indicate adjacent segments). Theoretically, all, or nearly all, action potentials will invade adjacent segments of the axon, providing a measure of the limitations of the frequency of activity that we can monitor with our methodology. **B.** Plot of the GCaMP6s activity observed in the two adjacent segments of the same axon in relation to walking and whisker motion energy. **C.** Expanded example of the measured activity in the two axon segments for detail. Note that the signal between adjacent segments is coherent at low frequencies, but not at higher frequencies. **D.** Coherence between segments of the same axon segments (N = 5 mice, n = 18 same-axon segment pairs) exhibit a high coherence at frequencies below approximately 1 Hz and a strong decrease at frequencies between 1 and 3 Hz, indicating that our monitoring methodology is limited to frequencies of approximately < 1 Hz. Comparison of coherence between all axon segments simultaneously monitored (N = 5 mice, n = 7272 pairs of axons) reveal a strong average coherence at frequencies less than 1 Hz, but this average coherence is lower than that for axon segments of the same axon. Plotting the distribution of average coherence at frequencies between 0.05 and 0.5 Hz reveals a broader distribution for heterogeneous axon segments in comparison to segments of the same axon. **E.** Comparison of coherence for adjacent segments of the same axon and all axon segments for noradrenergic axons (N = 4 mice, n = 30 same-axon segment pairs, n = 1699 different axon pairs). Plotting the distribution of low frequency coherence reveals a broader distribution for heterogeneous axon segments in comparison to segments of the same axon. **F, G.** The correlation in GCaMP6s signal between cholinergic (F) and noradrenergic (G) axon segments (signals low pass filtered at 1 Hz)

versus distance between the regions of interest containing the axon segments. 0 mm indicates axon segments within the same region of interest. Black squares represent correlation between adjacent segments of the same axon. Red dots illustrate the correlations between activity in all axon segments, excluding those that were clearly part of the same axon. Note that for both ACh and NA axons, there is generally a high correlation if the axon segments are adjacent and from the same axon (black squares). For all axon segments, the correlations are much more varied, ranging from around zero to greater than 0.8. These correlations drop only slightly with distance, even up to 4 mm, indicating that there is broad synchrony of cholinergic and noradrenergic axonal activity across the cortex. **H, I.** Plot of partial correlation versus ordinary correlation for cholinergic (H) and noradrenergic (I) axons reveals a strong contribution of a common signal to the correlations between most axon segments. The common signal was calculated as the average signal between all axon segments simultaneously imaged, excluding the two axon segments for which the partial correlation was calculated. Black dots represent segments of the same axon, which should exhibit a correlated signal that is independent of the common, group-average signal. **J.** Plot of the partial correlation, after removal of the common signal, with distance between axon segments. **K.** Difference between average partial and ordinary correlations between axon segments for periods including all data, no walking, no walking or whisking. A significant component of the common signal in partial correlations appears to be related to changes in behavioral state associated with bouts of whisking. *** = $p < 0.001$; ** = $p < 0.01$.

Relationship between VCIN activity and behavioral state

In addition to input from the basal forebrain, the cerebral cortex receives local cholinergic signaling through local VIP+/ChAT+ interneurons (VCINs). To determine whether activity in this population is modulated by arousal and behavioral state, we recorded GCaMP6s activity from the somata of ChAT-expressing cortical interneurons across the dorsal cortex while monitoring arousal related behavioral variables (whisker movements, walking; example shown in Fig. 5A-C). Cell bodies were selected for imaging from across the dorsal surface of the neocortex approximately 200 µm below the pial surface, consistent with VCINs being most densely present in cortical layers 2/3 (Dudai et al. 2021).

To determine whether VCIN activity tracked behavioral state transitions, we aligned GCaMP6s fluorescence in VCINs to the onsets and offsets of whisker movements (twitches or larger whisking bouts), and walking bouts (Fig. 5D-F, respectively). Averaged activity across all recorded VCINs tracked changes in the animal's behavioral state. Small whisker pad twitches were associated with a modest average increase in VCIN population activity, while longer whisking bouts and walking bouts were associated with larger increases in average population activity (Fig. 5D-F). In similarity with both BF-ACh and LC-NA axons, VCIN activity quickly increased at the onset of facial movements and returned to baseline within 1-2 s following a return to stillness (Fig. 5E). Examining the relationship between whisking onset and VCIN GCaMP6s activity at an expanded time base (Fig. 5E, inset) revealed a slight (< 150 msec) onset lag between whisking onset and VCIN GCaMP6s activity. VCIN activation was less tightly coupled to the onset and offsets of walking bouts (Fig. 5F), likely due to facial movements consistently occurring prior to walking bout onsets and persisting after walking offset (Fig. S2A,B). The observed relationship between VCIN signaling and whisking and walking behaviors was prominent in only a subset of these neurons (Fig. 5G-I). To quantify the reliability of responsiveness of individual VCINs to behavioral events, we calculated the probability that dF/F of a given VCIN was significantly increased 1 s following event onset, as compared to 1 s prior to event onset (Student's t-test, alpha = 0.01; Fig. 5J). On any given whisking bout 43.0 +/- 31.3% of VCINs responded significantly while on any given walking bout 27.2 +/- 27.9% responded significantly . Most cells responded more reliably to whisking bouts than would be expected by chance (distribution of the likelihood of significant response at randomly selected time points is shown in gray) while few cells showed a significant difference 1 second after walk onset versus 1 second prior.

To determine the extent to which VCIN signaling is uniform across cortical regions, we compared the correlation in activity across simultaneously imaged subpopulations (n = 4-15 cells per session; n = 178 total pairs) separated by a distance of up to 3.75 mm (Fig. 5K). Correlation of activity between pairs of VCIN neurons varied from 0.43 to 0.96 and averaged 0.74 +/- 0.12. As a control, we compared the correlation between GCaMP6s signaling in two halves of the same VCIN neurons (Fig. 5K, black dots). We reasoned that any correlation below 1 would reveal limitations within our data set. Indeed, all (n = 18) of the adjacent cell body halves exhibited a correlation at, or near, 1 (minimum correlation = 0.91; Fig. 5K). These correlations are higher than those we obtained by comparing two segments of the same axon (e.g. cf. Figs. 4F, 5K). We assume this difference is the result of the high dF/F signals, and larger imaging volumes, exhibited by cell bodies in comparison to axon segments. There appeared to be no significant relationship between distance and correlation between VCIN GCaMP6s activity (Fig. 5K).

To examine the possibility that correlations between VCIN neuronal GCaMP6s signal was the result of co-correlation with a common variable, related to behavioral state, we performed partial correlations in which the common signal was the average VCIN activity of simultaneously imaged neurons (excluding the two cells being correlated; Fig. 5L). For neurons with ordinary correlations less than approximately 0.6, the residual partial correlation centered around approximately 0, suggesting that these neurons were correlated in their activity owing to co-correlation with a common signal. Closer examination of the subset of pairs of neurons that exhibited ordinary correlations greater than approximately 0.6 revealed a population of neuronal pairs whose partial correlation was unusually positive, increasing towards a partial residual correlation of 0.84, as the ordinary correlation approached 0.96 (Fig. 5L). This result suggests that this small number of neuronal pairs were strongly correlated in activity outside that associated with the common (average) VCIN activity.

Calculating partial correlation between two halves of the same cell body, taking into account the average common activity of other simultaneously imaged neurons, did not reduce the correlation in VCINs (ordinary correlation: 0.99 +/- 0.02, partial correlation: 0.99 +/- 0.03; $t = -1.35$, $p = 0.20$), an expected result since these two cell body halves should be highly correlated in all of their activity, including that remaining following removal of the common signal correlation. Plotting the partial residual correlation between VCIN neurons as a function of distance revealed a small decrease with distance ($r = -0.14$; $p < 0.01$), suggesting that nearby VCIN neurons are slightly more likely to be correlated outside the common signal than distant cells. Interestingly, in contrast to ACh axons, the reduction in correlation between VCIN neurons by taking into account a common signal was not dependent upon whisking or walking (Fig. 5N).

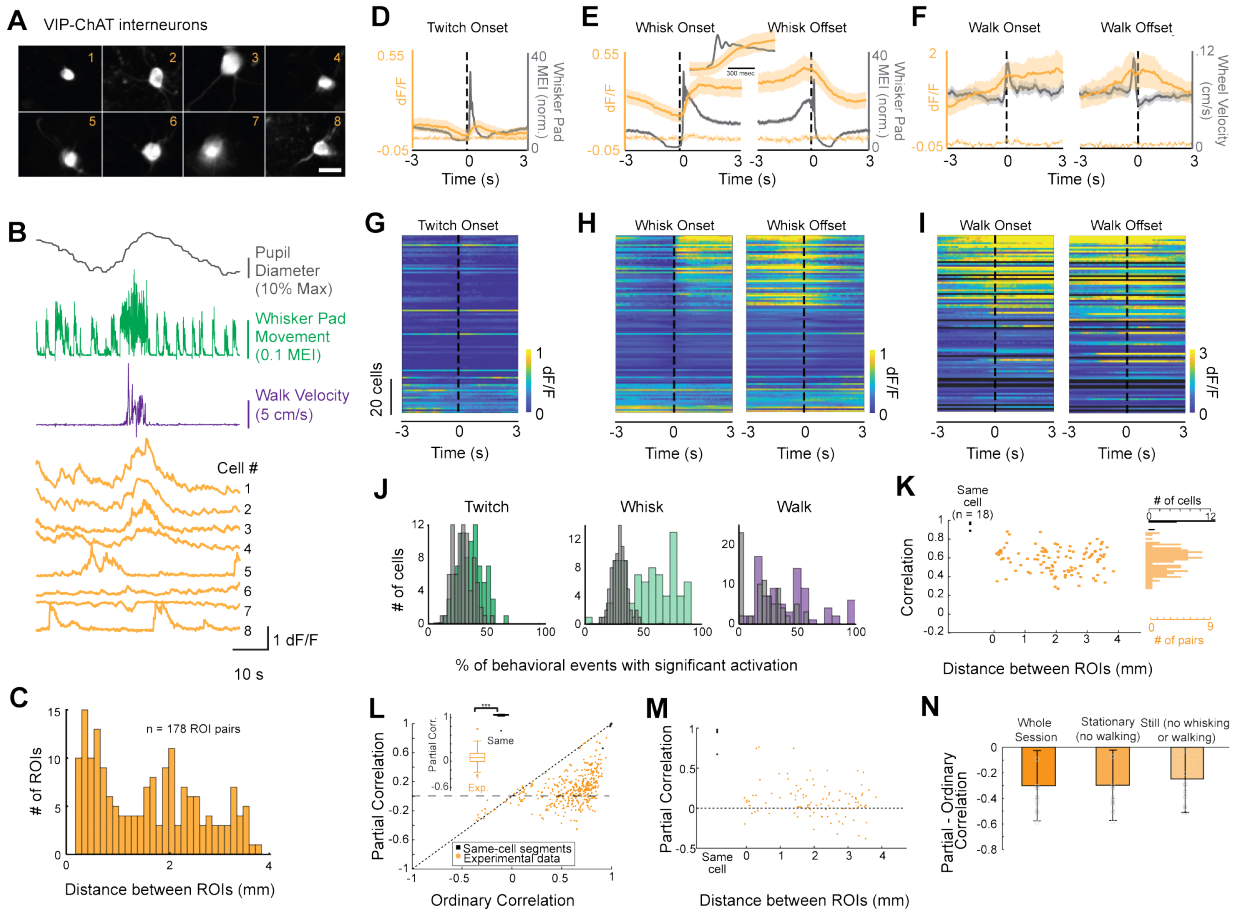

Figure 5. A subpopulation of VIP-ChAT cortical interneurons track changes in behavioral state. A. Images of 8 simultaneously recorded VIP-ChAT cortical interneurons (VCINs). **B.** Example recording taken from the 8 somas shown in panel A. Note the clear heterogeneity of VCIN response (yellow) during walking (purple) and whisking (green) activity. **C**. Distribution of distance between ROIs containing VCINs. ROIs were separated from 0.075 to 3.9 mm (N = 7 mice, n = 98 cells). **D-F.** Group averaged VCIN activity aligned to 870 twitching onsets, 1104 whisking onsets, 1015 whisking offsets, and 127 walking onsets and offsets (N = 6 mice, n = 84 cell bodies for walking data). Gray traces show the averaged change in whisker pad motion energy (D,E) or walking speed (F). Dotted lines represent autofluorescent blebs. Inset in E is at an expanded time base with normalization of data from base to peak for comparison of the kinetics of onset of whisker movements and VCIN activity. **G-I.** Same data as displayed in panels C-E, but separated to visualize heterogeneity of individual cell responses to behavioral state changes. Cells are sorted based on the magnitude of dF/F change at the onset of whisking. **J.** The consistency of a single VCIN's response to behavioral state changes was quantified by calculating the percent of twitching, whisking, or walking bouts that were associated with significant increases in dF/F and compared to distributions attained with shuffled data. **K.** Correlation between VCIN cells by distance between the ROIs. Measuring GCaMP6s from two halves of the same cell body resulted in an average correlation that was near 1 (black dots; N = 3 mice, n = 18 same-cell pairs). **L.** Partial residual correlation (following removal of correlation with common signal) versus ordinary correlation reveals that a significant component of the correlation results from the common signal. Common signal was calculated as the average activity of the imaged neurons, excluding the two cells being correlated. *** = $p < 0.001$. **M.** Partial residual correlation as a function of the distance between ROIs containing the cells being correlated. The partial correlation decreases slightly with distance ($r = -0.09$; n= 98 cells; $p = 0.07$). **N.** Effect of restricting data to stationary or still periods on partial correlations.

Discussion

In this study, we used GCaMP6s calcium imaging in cholinergic and noradrenergic cortical axons to determine the extent to which each neuromodulatory pathway may provide a global state-dependent signal to cortical regions, and whether or not other, more heterogeneous, activity may also be present. First, our results confirmed that BF-ACh and LC-NA activity across the cortex is strongly linked to changes in behavioral state, as indicated by externally observable measures (whisker/facial movements, locomotion, and pupil diameter) with strong ACh/NA activations occurring during periods of behavioral engagement (Figs. 1-4, S1, S2). Second, we found that facial/whisker movement is a better predictor of BF-ACh and LC-NA activity than walking speed or pupil diameter (Fig. 3). Third, we found evidence for heterogeneous ACh and NA axonal signaling (Fig. 4, S1K-O). Finally, we presented evidence for both behavioral and heterogeneous cortical ACh signaling via local VIP-ChAT interneurons (Fig. 5).

Cholinergic and noradrenergic signaling related to arousal and behavioral engagement

BF-ACh and LC-NA have long been implicated in initiating and maintaining the waking state and arousal (Picciotto, Higley, and Mineur 2012; McCormick 1989; Berridge 2008). Early work exploring the role of the noradrenergic neurons of the locus coeruleus (LC) strongly suggested that this region is important for triggering sleep-wake transitions and variations in behavioral engagement and vigilance. For example, activity of LC neurons is higher during waking compared to sleeping (Hobson et al. 1975), and increased LC activity occurs before the transition from sleep to awake (Aston-Jones and Bloom 1981). The potential causal role of the LC in regulation of wakefulness is supported by more recent experiments that have shown that optogenetic stimulation of the LC induces a sleep-wake transition (Carter et al., 2010; Hayat et al., 2019). Noradrenergic signaling is also associated with moment-to-moment fluctuations in arousal and behavioral engagement/vigilance within the waking state (Joshi et al. 2016; Joshi and Gold 2022; reviewed in Poe et al. 2020; Aston-Jones and Cohen 2005). In the mouse, activity of noradrenergic axons in primary visual and auditory cortices tracks fluctuations in pupil diameter and orofacial movements (Larsen and Waters 2018; Reimer et al. 2016), which, in mice, are indicators of behavioral state (reviewed in McGinley et al. 2015). Moreover, optogenetic activation of the LC induces pupil dilation while inhibition of the LC leads to pupil constriction (Reimer et al. 2016; Megemont, McBurney-Lin, and Yang 2022; Breton-Provencher and Sur 2019). Early recordings from the LC in awake, behaving rodents or monkeys revealed tonic increases in average firing rate related to arousal and phasic, often synchronous, discharge associated with short-term increases in behavioral vigilance to external environment and stimuli (reviewed in Aston-Jones and Cohen 2005; Sara and Bouret 2012; Sara 2009). More recent investigations reveal at least some degree of heterogeneity and specialization in LC neuronal signaling (see below; Poe et al. 2020; Totah, Logothetis, and Eschenko 2019; Breton-Provencher et al. 2022; Uematsu et al. 2017; Chandler, Gao, and Waterhouse 2014). Our observation of a common signal across noradrenergic axons related to behavioral state (e.g. whisker movements - a general measure of behavioral engagement in mice), is consistent with a global noradrenergic influence on cortical and subcortical network activity related to behavioral arousal, engagement, and vigilance.

Similar to the LC, the basal forebrain cholinergic system has been associated with transition to the waking state from sleep (Xu et al. 2015; Han et al. 2014; Irmak and de Lecea 2014; Teles-Grilo Ruivo et al. 2017) as well as general cortical activation (Buzsaki et al. 1988; Metherate and Ashe 1993; Metherate, Cox, and Ashe 1992). During slow wave sleep, ACh release in the cortex and thalamus is substantially reduced compared to the waking state and REM sleep state (M. G. Lee et al. 2005; Williams et al. 1994) and stimulation of the cholinergic basal forebrain promotes wakefulness (Zant et al. 2016; Han et al. 2014; Xu et al. 2015). In the waking state, cortical cholinergic axonal activity fluctuates in relation to increases in behavioral arousal and engagement (as measured by the onset of whisker movements, increases in pupil diameter and locomotion; (Nelson and Mooney 2016a; Reimer et al. 2016; Eggermann et al. 2014). Activation of the basal forebrain cholinergic system appears to be particularly important for the suppression of spontaneous slow oscillations in cortical and thalamocortical activity, which are characteristic of behavioral quiescence or drowsiness (Eggermann et al. 2014). Our observation of a global common signal in cholinergic axons correlated with measures of behavioral engagement, particularly movements of the whiskers and face, support the view that one of the major roles of the basal forebrain cholinergic system is to provide a broad modulation of the neocortex in association with moment-to-moment changes in behavioral state, including arousal, engagement, vigilance, and attention. Interestingly, a recent study of dopaminergic axons within the mouse cortex also revealed state-dependent activity very similar to that observed here for cholinergic and noradrenergic axons, including increases in activity with whisker movements, pupil dilations, and locomotion (Fig. 4 in Sturgill et al. 2020). These results, along with studies of multiple cell types throughout the cortex, thalamus, and other structures (McGinley et al. 2015; McCormick, Nestvogel, and He 2020; Stringer et al. 2019; Musall et al. 2019; Steinmetz et al. 2019), reveal frequent coordinated rapid shifts in neural dynamics throughout the mouse brain during the waking state that are highly coordinated with rapid changes in behavioral state (see below).

Are Cholinergic and Noradrenergic Systems Driving, or are they Driven by, Rapid Waking State Transitions?

Extracellular, intracellular, and optical recordings from a wide variety of cortical (and subcortical) neurons, both excitatory and inhibitory, reveal marked and rapid transitions in neural network dynamics that mirror those occurring in the behavioral state of the animal (McGinley et al. 2015; Reimer et al. 2014; Vinck et al. 2015; Niell and Stryker 2010; Nestvogel and McCormick 2022; Steinmetz et al. 2019; Stringer et al. 2019; Musall et al. 2019; Sachidhanandam et al. 2013; reviewed in McCormick, Nestvogel, and He 2020; McGinley et al. 2015; Poulet and Crochet 2018; Petersen 2019). Head fixed mice can exhibit a state of behavioral quiescence, characterized by stillness, the lack of orofacial movements, and a constricted pupil diameter. This state of quiescence is often punctuated by brief (e.g. < 1 sec) periods of whisker movements accompanied by small pupil dilations, and often body twitches. These brief pupil dilations, which are often, but not always, associated with whisker/body movements, have been termed microarousals and are associated with a striking depolarization of many cortical pyramidal cells (McGinley, David, and McCormick 2015; Nestvogel and McCormick 2022). Transitions to more prolonged and larger forward-backward swings of the whiskers (i.e. whisking), may also occur and may or may not be followed by a transition to full locomotion (e.g.

Fig. 1). These behavioral states are closely aligned to changes in neural dynamics in cortical, thalamocortical, and other brain systems, suggesting that the entire mouse (from cortex to brainstem; from nose to tail) is undergoing frequent and rapid state-transitions, whether or not the mouse is in the “resting” awake state, or performing a trained sensory detection/discrimination task (McGinley et al. 2015; Reimer et al. 2014; Vinck et al. 2015; Niell and Stryker 2010; Nestvogel and McCormick 2022; Steinmetz et al. 2019; Stringer et al. 2019; Musall et al. 2019; Sachidhanandam et al. 2013; reviewed in McCormick, Nestvogel, and He 2020; McGinley et al. 2015; Poulet and Crochet 2018; Petersen 2019). At the cortical and thalamocortical level, the resting, behaviorally quiescent state, is characterized by the appearance of spontaneous rhythms similar to slow-wave and alpha rhythms that are generated through local circuit and thalamocortical neuronal, synaptic, and network properties. The transition to whisker twitches, full whisking, or locomotion, are all associated with a striking and rapid (tens of msec) depolarization of many excitatory neurons, most likely throughout the cortex and thalamus (Nestvogel and McCormick 2022; Petersen 2019; Poulet and Crochet 2018). These behavioral and cortical/thalamocortical neuronal network state-transitions are accompanied by equally striking changes in the activity of cortical cholinergic, noradrenergic, and perhaps dopaminergic (Sturgill et al. 2020) neuromodulatory systems (Eggermann et al. 2014; Larsen and Waters 2018; Reimer et al. 2016; Nelson and Mooney 2016a; Lohani et al. 2021). Given that the release of norepinephrine and acetylcholine can have potent influences on the state of activity in cortical and thalamic neurons and networks (McCormick, Nestvogel, and He 2020; McCormick 1992), the question then becomes: are the state transitions in neural networks driving the general changes in cholinergic and noradrenergic activity, are they the consequence of changes in these neuromodulatory systems, or perhaps both?

One of the striking features of state-transitions from behavioral quiescence to engagement in mice is the rapidity with which thalamocortical networks are affected by the onset of movement (tens of msec or less; (Nestvogel and McCormick 2022). These rapid state transitions appear as strong depolarizations of both cortical and thalamic neurons, and the kinetics of these depolarizations are indicative of mediation through ionotropic receptor-mediated synaptic transmission, both in the neocortex and thalamus (Nestvogel and McCormick 2022). Indeed, pharmacological block of thalamic activity results in a near complete block of movement-related sustained depolarization of both visual and somatosensory cortical neurons, suggesting that barrages of synaptic activity arriving from increased activity in the thalamus are critical to the sustained depolarization of cortical networks during behavioral engagement (Eggermann et al. 2014; Nestvogel and McCormick 2022). In the presence of thalamic inactivation, the transition from behavioral quiescence to movement (e.g. whisking), results in a suppression of ongoing slow-rhythm activity in cortical networks and this effect is blocked by application of a combination of cholinergic nicotinic/muscarinic receptor antagonists. Importantly, activation of the cortical cholinergic axons in the presence of thalamic inactivation also results in a suppression of ongoing slow rhythms in cortical neurons, without the generation of a depolarization (Eggermann et al. 2014). Thus, the transition from behavioral quiescence to engagement/movement appears to initiate the transition from lower frequency spontaneous cortical/thalamocortical oscillations to sustained depolarization and activation through at least

two mechanisms - cholinergic suppression of ongoing activity and thalamic sustenance of prolonged depolarization during behavioral engagement/movement.

While some studies have suggested that the activation of noradrenergic receptors may be critical to the transition of cortical networks from slow wave-like activity during quiescence to the sustained activity of behavioral engagement (Polack, Friedman, and Golshani 2013), the slow (hundreds of msec to seconds) nature of noradrenergic effects, which operate through g-proteins/second messenger pathways, would seem to preclude this neuromodulatory system in mediating the more rapid kinetic components of these transitions (even though the activation of noradrenergic fibers appears to be rapid during the initiation of movements; Fig. 2B). In contrast, cholinergic systems can rapidly depolarize cortical excitatory and inhibitory neurons through the activation of nicotinic receptors, suggesting that this signaling mechanism may contribute to the rapid transitions from inactive to active cortical and thalamocortical states (Nelson and Mooney 2016a; Fu et al. 2014). Indeed, it has been suggested that cholinergic activation of VIP-interneurons through nicotinic receptors, resulting in the disinhibition of pyramidal neurons, is the main mechanism by which behavioral engagement enhances cortical responsiveness (Fu et al. 2014). This proposal, however, is inconsistent with the finding that inactivation of the thalamus results in a profound suppression of activation of the cortex with behavioral engagement (Eggermann et al. 2014; Nestvogel and McCormick 2022). The excitation of VIP interneurons through cholinergic activation of nicotinic receptors could contribute to movement-related suppression of on-going slow-wave oscillations. The inhibition of layer 4 neurons, or the suppression of synaptic transmission through pre-synaptic actions of acetylcholine, are two other possibilities (reviewed in Poulet and Crochet 2018).

From these considerations, we hypothesize that the rapid activation of cholinergic and noradrenergic systems in the transition from behavioral quiescence to movement/engagement is *not* the main driver of the rapid activation of cortical and thalamocortical networks, but rather contributes to slower, perhaps more prolonged, adjustments in network activity and neuronal excitability/responsiveness as appropriate for behavioral state. The detailed nature of these modulations remain to be determined, but appear to operate through both a global, common signal, as well as a more heterogeneous, perhaps spatially and temporally precise mechanism (e.g. Poe et al. 2020; Totah et al. 2018).

<u>Heterogeneous ACh and LC-NA signaling</u>

In addition to a global behavioral state-linked signal, ACh and LC-NA may also provide heterogeneous signals throughout the brain. These targeted signals may support a range of brain processes and behaviors, including selective sensory processing, cortical plasticity, and memory formation (Janitzky et al. 2015; Aston-Jones and Cohen 2005; Sara 2009; Sara and Bouret 2012; Usher 1999; Deitcher et al., 2019; Breton-Provencher et al. 2022; Uematsu et al. 2017; Polack, Friedman, and Golshani 2013; Pinto et al. 2013; Nelson and Mooney 2016a; Goard and Dan 2009; Ego-Stengel et al. 2001).

Specificity of cholinergic cortical signaling has been demonstrated both anatomically and functionally. Inputs and outputs of cholinergic neurons in the BF are topographically organized

(Zaborszky et al. 2015; Gielow and Zaborszky 2017) and activating distinct regions of the BF results in desynchronization of restricted cortical regions (Kim et al. 2016). Recent work has demonstrated heterogeneity in cortical ACh receptor activation, particularly during periods of locomotion (Lohani et al. 2021; Howe et al. 2019), and ACh receptor subtype distribution is highly non-uniform across the brain (Picciotto, Higley, and Mineur 2012). Simultaneous monitoring of activity of cholinergic neurons in different parts of the basal forebrain system during the learning and performance of a variable reinforcement task in mice reveal both broadly coordinated activity as well as consistent differences in the patterns of cholinergic neuronal activity in relation to their projection targets (Robert et al. 2021).

The extent to which the LC-NA system is modular, or provides targeted neuromodulation throughout the brain, remains under debate, although evidence for modularity is accumulating (Poe et al. 2020; Totah et al. 2018; Uematsu et al. 2017; Breton-Provencher et al. 2022; Totah, Logothetis, and Eschenko 2019; Chandler et al. 2019). While some anatomical and functional evidence supports the view that neurons within the LC-NA system share a broadly similar connectivity and functional effect, and that the activity of LC neurons are often synchronized (Schwarz et al. 2015; Kim et al. 2016; Deitcher et al., 2019), more recent investigations have emphasized the presence of genetic, anatomical, and functional specializations within sub-regions of the locus coeruleus (reviewed in Poe et al. 2020; Totah et al. 2018). Indeed, two recent reports on the activity and influence of subregions of the LC in mice performing learned tasks provide evidence for both broad correlated NA coordination, as well as functional specialization between different neuronal groups within the LC (Breton-Provencher et al. 2022; Uematsu et al. 2017).

Our data is consistent with the LC-NA and BF-ACh systems broadcasting both a broad state-dependent signal over wide regions of the neocortex, as well as more heterogeneous activity that may be regionally or temporally separate and distinct. Evidence supporting the presence of a broadly coordinated signal is the high degree of correlation between the GCaMP6s activity in axonal segments and the large effect on this correlation of taking into account the partial correlation with the average signal of other axons that were simultaneously recorded (e.g. Fig. 4). Evidence for a more heterogeneous signal is provided by the large range of correlations and coherences between axonal segments, which is much broader than correlations/coherences between axon segments of the same axon. In other words, the broad population of axon segments do not behave as if they are all carrying the same activity, which is the case when comparing segments from the same axon (Fig. 4). In addition, taking into account the common average signal of simultaneously imaged axons leaves a broad distribution of both positive and negative correlations between axon segments that are either close or distant, suggesting that these sub-clusters of NA and ACh axons may be coordinated in their activity at a level beyond that associated with the common signal of behavioral state (Fig. 4).

<u>ACh signaling from cortical interneurons</u>

ACh signaling is complicated by the presence of two distinct cholinergic systems that modulate activity in the cortex: the well-characterized long-range projections from the BF discussed above and a population of cortical interneurons (VCINs) that are equipped to

modulate local cortical circuits through both GABAergic and cholinergic signaling. VCINs are functionally and spatially situated as a prime candidate to enhance regionally specific modulatory signaling of the cholinergic system. VCINs have been reported to be sparsely distributed throughout the cortex, primarily in layers 2/3 (Dudai et al., 2020) and they possess a combination of GABAergic and cholinergic axon terminals, arranged in a highly target-specific manner, ideal for circuit specific modulation. Individual axon segments of VCINs can contain both VAChT+ and VAChT- terminals, suggesting specificity based on post-synaptic targets (Dudai et al. 2021; Obermayer et al. 2019; Granger et al. 2020).

The present work provides evidence that, like the long-range cholinergic BF projections to cortex, some local VCINs track the arousal and behavioral state of the animal, exhibiting increased activity related to behavioral state changes (Fig. 5C-E). However, amongst the population of VCINs, there is heterogeneity in the cells' responsiveness to behavioral state, with only a subset of VCINs across the cortex displaying activity that strongly and reliably tracks behavioral state variables (Fig. 5B, F-I). This heterogeneity of activity within local cholinergic signaling may reflect circuit-specific arousal-related modulation of cortical dynamics, or it may be evidence that there is a functionally distinct subgroup of VCINs, which are less strongly influenced by behavioral/arousal state changes.

Conclusions

Together, our findings provide evidence that activity within cholinergic and noradrenergic cortical projections is tightly coupled to spontaneous behavioral state changes. By simultaneously imaging axonal activity across functionally distinct cortical areas separated by up to ~4 mm, we demonstrate that both BF-ACh and LC-NA projections provide a global, arousal/behavioral state-related signal to the neocortex. Notably, our data suggest that heterogeneous signaling may also be provided by both BF-ACh and LC-NA projections and, in addition, by local cortical cholinergic interneuron activity.

Supplemental Figures

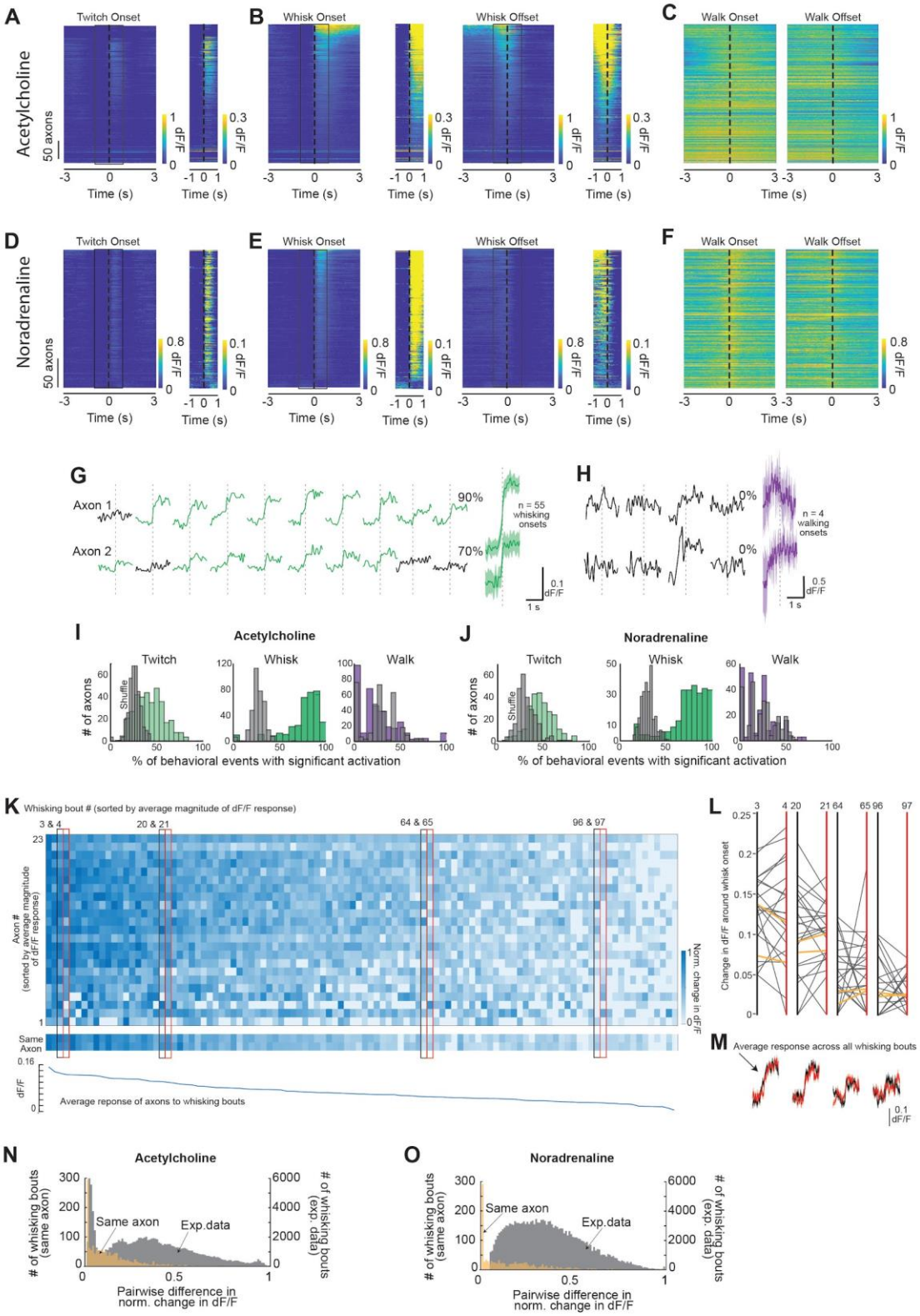

Figure S1. Individual axonal responses to behavioral state changes. Relates to Figures 1 and 2. **A-F.** Same data as displayed in Fig. 2A-C, but separated to visualize heterogeneity of individual axon responses to behavioral state changes. Axons are sorted based on the magnitude of dF/F change at the onset of whisking. For A, B, D and E, two scales of dF/F are shown for clarity. **G, H.** Example raw traces of axon segments illustrating the probability that the axon segment showed a significant response in relation to the onset of a bout of whisking (G) or the onset of wheel movement (H). Green traces were those detected to have a significant response on that trial. Black traces did not. In this illustration, Axon 1 exhibited 90% probability of significant activation with whisking, but 0% chance that the 1 second after onset of walking was significantly different than the 1 second prior to walking onset. Axon segment 2 showed a 70% probability or significant response to onset of whisking and a 0% rate of difference for GCaMP6s average signal difference during the 1 second following, versus preceding, walk onset. **I,J.** Probability that a given BF-ACh or LC-NA axon will increase fluorescence alongside the onset of a twitch, whisk, or walking bout (1 second after vs. 1 second before onset). Gray bars are the distribution resulting from a shuffle (see Methods). Responsiveness from n = 397 axons (N = 5 mice) was measured at the onset of 1108 twitches, 330 whisking bouts, and 101 walking bouts for ACh (I). Responsiveness from n = 283 axons (N = 6 mice) was measured at the onset of 644 twitches, 400 whisking bouts, and 34 walking bouts for NA (J). **K.** Representative example of axonal activity at the onset of whisking bouts. Darker colors represent a stronger activation around whisking onset (determined by subtracting mean dF/F during 1 s prior to whisking onset from mean dF/F of 1 s following whisking onset and normalizing across all whisking bouts). To visualize activity of axons around whisking bouts of similar magnitude, the plot is sorted horizontally by average magnitude of axonal responses to each whisking bout. Axons are shown from highest average responsiveness to whisking (top) to lowest (bottom). Note that some axons respond oppositely to whisking bouts of similar magnitude (pairs of examples shown in black and red boxes). Middle: Same analysis for two segments of the same axon recorded during this example session. Note the relative uniformity of responses between these same-axon segments compared to the heterogeneity shown across all recorded axons. Bottom: average change in dF/F across all simultaneously recorded axons at the onset of whisking bouts. This metric was used to sort across whisking bouts. **L.** Change in dF/F at the onset of whisking bouts of similar magnitude. Examples are taken from whisking bouts boxed in (K). Yellow lines represent changes in dF/F of the two same-axon segments. Segments of the same axon generally respond similarly to whisks of similar magnitude while there is a clear diversity in response across all 23 recorded axons. **M.** Averaged dF/F of all recorded axons around the onset of whisking bouts. Color of the dF/F trace corresponds to the color of the box in (K) and the vertical lines in (L). **N-O.** Comparison of pairwise differences in normalized change in dF/F between all simultaneously imaged axon segments for each whisking bout. For both BF-ACh (N) and LC-NA (O), the distribution of differences between activation amplitudes between pairs of heterogeneous axon segments was more broadly distributed than for segments of the same axons. For ACh, N = 5 mice, n = 7272 different axon pairs and n = 18 same axon pairs. For NA, N = 6 mice, n = 1699 different axon pairs and n = 30 same axon pairs.

Fig. S2

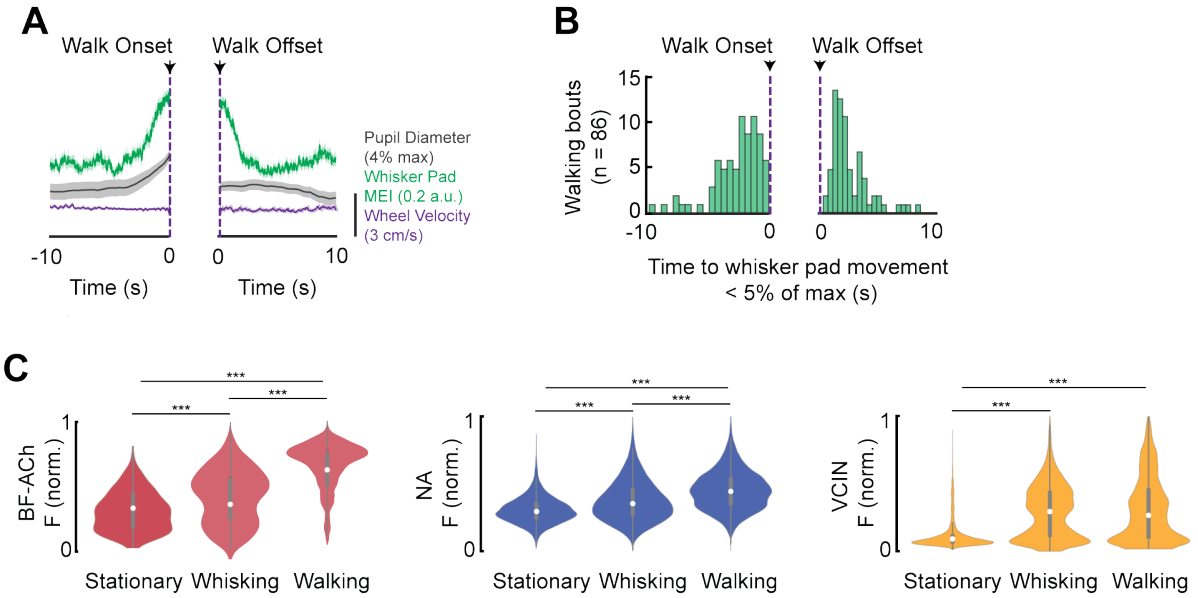

Figure S2 Variable timing of onset/offset of whisking and walking and fluorescence of cholinergic and noradrenergic axons and VCINs during different states. Related to Figure 2. **A.** Average whisker movements and pupil diameter preceding

and following the onset/offset of a walking bout (n = 86 walking bouts). Note that the average movement in the whisker pad both precedes, and follows, walk onset by several seconds. **B.** Distribution of onset/offset of bouts of whisker movements to the onset/offset of a bout of walking. Note that whisker movement onset/offset is variable in comparison to walking onset/offset, and distributed over several seconds. **C.** Violin plots of the fluorescence of cholinergic (n = 397), noradrenergic (n = 283) axons and VCIN (n = 98) neurons during the different behavioral states of stationary (no detected whisker movements or walking), whisking (twitching or whisking) and walking. Note the variations in the magnitude of fluorescence recorded in each population across behavioral states. *** $p < 0.001$.

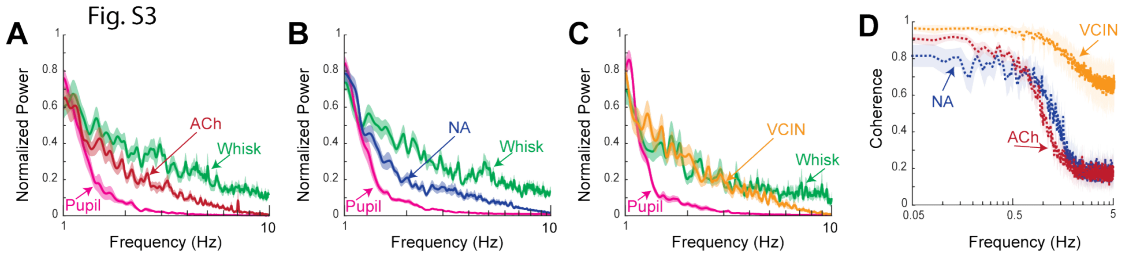

Figure S3. Distribution of power and coherence for pupil, cholinergic, noradrenergic, whisking, and VCIN. Related to Fig. 3C, D. **A.** Power distribution between 1 and 10 Hz for cholinergic axon fluorescence, pupil diameter, and whisker pad motion energy. N = 5 mice, n = 397 axons. **B.** Same as A but including noradrenergic axons. N = 6 mice, n = 283 axons. **C.** Same as A, B but showing VCIN. N = 7 mice, n = 98 cells. Note that whisker pad motion energy and VCIN fluorescence has more power at frequencies above approximately 1.5 Hz than cholinergic or noradrenergic axons. **D.** Coherence between adjacent portions of the same ACh, NA axons or segments of the came VCIN cell body. Note the large fall off of coherence for frequencies above approximately 1 Hz. The fall off for power for VCIN neurons is less marked.

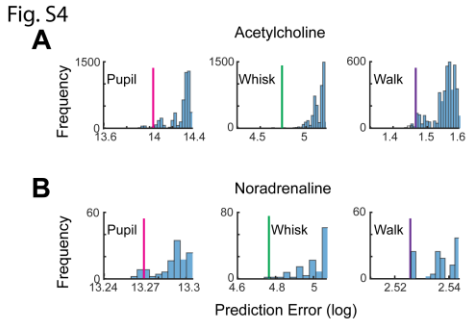

Figure S4. Quantification of linear regression predictive error. Related to Figure 3F and H. Prediction error associated with matched behavior and axon imaging recordings (solid lines) and all permutations of unmatched recordings (blue bars).

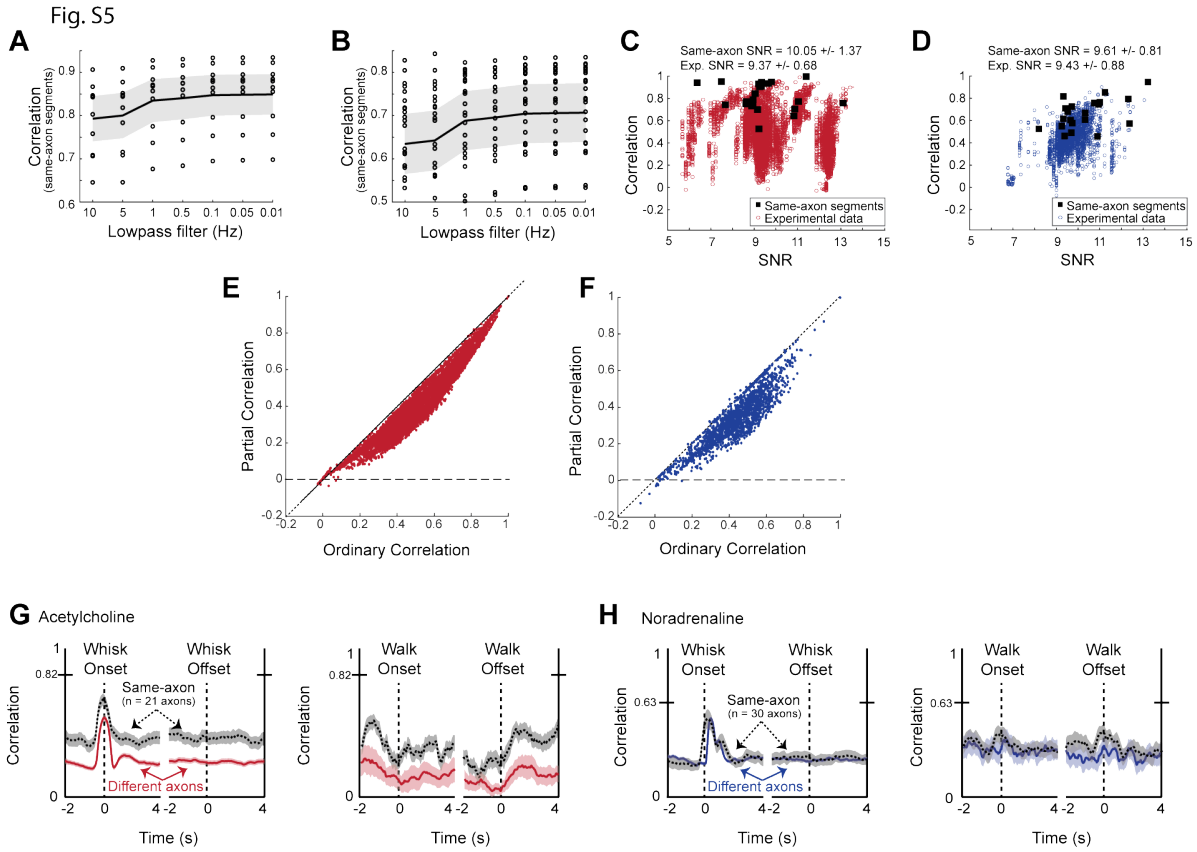

Figure S5. Features of axonal imaging data relevant to interpreting imaging results. Related to Fig. 4. **A.** Effect of applying low pass filters with different cut off frequencies on the average correlation between cholinergic axon segments. A small increase in correlation was obtained by applying low pass filters of 1 Hz or lower. **B.** Same as A, except for noradrenergic fibers. **C.** Comparison of correlation and signal-to-noise (SNR) ratio for same axon segments (black squares) and complete data set (red dots). Correlations for axon segments from the same axons were higher than for the complete data set, even though the SNR was similarly distributed. Correlations did not correlate with SNR. **D.** Same as C, except for noradrenergic fibers. **E, F.** Partial correlations versus ordinary correlations in which the common signal was whisker pad motion energy. Note that the partial correlation was consistently lower than the ordinary correlation for both ACh and NA, but that the effect was less pronounced than that obtained when the average dF/F was the common signal (Fig. 4 H-I). **G.** Average correlation between BF-ACh axon segment pairs aligned to the onset and offset of whisker pad motion and walking exhibit a transient increase at whisker movement onset. However, this transient increase is equally prominent for the two segments of the same axon, indicating that it is a consequence (artifact) of the imaging methodology. **H.** Same as G, except for NA axon segments.

Video S1. Example of mouse face during twitching, whisking, and walking. Related to Figs. 1 and 2. Video recording of a mouse's face during periods of twitching, whisking, and walking. Note the difference between a short (< 0.5 s) twitch and a sustained (> 1 s) whisking bout. Also note the prominent whisker pad motion during bouts of walking.

Video S2. Axon imaging and behavioral acquisition methodology. Related to Fig. 1. A headpost was implanted on the skull overlying the dorsal cortex (top of video = anterior). Cortical regions coarsely aligned to the Allen Brain Institute Common Coordinate Framework are shown for reference. An 8 mm circular cranial window was placed over multiple cortical regions. In each imaging session, axons or cells within up to a 5x5 mm region could be imaged simultaneously. An epifluorescence image of the visible brain areas for this example session is shown along with four red squares, which indicate the position of each of 4 ROIs recorded simultaneously. Next, all collected data are shown for this example session. Top left: position of regions of interest. Top middle: video recording of the mouse's face (used for pupil diameter and whisker pad motion extraction). Bottom left: traces of dF/F for each isolated axon shown on the right along with whisker pad motion energy, walking speed, and pupil diameter. Right: 4 videos of ACh axon imaging aligned in time to behavioral variables shown on the left. Videos are sped up by 10x but are otherwise unprocessed (i.e. no motion correction or temporal resampling). The pupil is large in this video owing to low UV/white light levels to enhance axon imaging SNR (see Methods).

Materials and Methods

Animals

All experiments were approved by the University of Oregon Institutional Animal Care and Use Committee. Experiments were conducted using male and female mice aged between 6 and 10 weeks at study onset. All mouse strains used in this study were of C56BL/6J (IMSR Cat# JAX:000664, RRID: IMSR_JAX:000664) background and were purchased from Jackson Laboratory and bred in-house. ChAT-cre mice (IMSR Cat# JAX:006410, RRID: IMSR_JAX:006410), which express cre-recombinase in cholinergic neurons, were used for viral injection experiments to record from BF-ACh projections. Viral injections were used for BF-ACh studies to avoid imaging axons or dendrites from cholinergic projections not arising from the BF (e.g. VCINs). For LC-NA experiments, DBH-cre mice (IMSR Cat# JAX:033951, RRID: IMSR_JAX:033951), which express cre-recombinase in noradrenergic neurons, were crossed with Ai162 (IMSR Cat# JAX:031562, RRID: IMSR_JAX:031562) mice, which cre-dependently express GCaMP6s. ChAT-cre mice crossed with Ai162 mice were used for VCIN studies, since these mice express GCaMP6s in all cholinergic cells and projections, including VCINs. All mice were individually housed under an inverted 12:12 hr light/dark regime, and had access to food and water *ad libitum*. All experiments were conducted during the active dark cycle in reverse light-cycled mice.

Surgical Procedures

All surgical procedures were performed in an aseptic environment under 1-2% isoflurane anesthesia (oxygen flow rate: ~1.5 L/min) and mice were homeothermically maintained at 37.5°C under systemic analgesia (Meloxicam SR: 6 mg/kg, s.c.; Buprenorphine SR: 0.05 mg/kg, s.c.). For viral injection experiments, two small craniotomies (~1mm) were made for bilateral viral injections into the basal forebrain (from bregma: 1.44 mm lateral, 0.6 mm posterior). The pipette was lowered 3.8 mm ventral to the surface of the brain and approximately 1 µl of an axon-targeted GCaMP6s adeno-associated virus (pAAV-hSynapsin1-FLEx-axon-GCaMP6s, addgene) solution was injected. Animals were allowed to recover from the viral injection surgery before any subsequent surgeries. Imaging was performed at least 3 weeks after virus injection to allow adequate time for axonal transport to the cortex.

For 2-photon imaging a titanium headpost was affixed to the skull with dental cement after removing the overlying skin and fascia. Then, an 8 mm circular craniotomy was made overlying the dorsal cortex using a dental drill. An 8 mm circular glass coverslip was placed in the craniotomy and the coverslip was affixed to the skull with flow-it composite (Flow-It ALC, Pentron) and a thin layer of dental cement. After all surgeries, mice recovered in a ~90° F recovery chamber and post-operative subcutaneous lactated ringer's solution was administered for 1 – 3 days, as required.

Experimental Design

Arousal Measures

For all experiments mice were head-fixed atop a cylindrical running wheel and video of the mouse face was acquired at 30 Hz using a Teledyne camera. Pupil diameter was measured both in real-time and offline using a custom labview script. Running speed was measured using a rotary encoder (McMaster-Carr) attached to the wheel. The running wheel was supported by springs and the rotary encoder also detected vertical movements of the running wheel, which can occur both, and between, bouts of running. Whisker-pad movement was measured by selecting a region of interest over the whisker pad and calculating the motion energy index (MEI) across the video. Motion energy index was defined as the sum of the absolute change in pixel intensity within the ROI between adjacent video frames. All waveform and trigger signals were digitized through a Micro1401 or a Power 1401, and collected using Spike2 version 7 or 8.

2-photon Imaging

2-photon imaging was conducted using a ThorLabs Multiphoton Mesoscope (Excitation NA 0.6, Collection NA 1.0) equipped with a 12 kHz Resonant Scanner and Virtually Conjugated Galvo Scanner Set along with a 1 mm range Remote Focusing Unit, allowing for rapid imaging across multiple ROIs varying in X, Y, and Z coordinates simultaneously (Sofroniew et al. 2016). Excitation of GCaMP was achieved via a Ti-sapphire laser tuned to 920 nm (MaiTai, Spectra Physics). Scan Image software (Vidrio) was used for all imaging sessions. For cell body imaging a minimum resolution of 0.5 μm/pixel was used and for axonal imaging a minimum resolution of 1 μm/pixel was used to clearly delineate borders of somas or axonal processes. Fields of view ranged between 50x50 and 400x400 μm and were obtained at a minimum frequency of 10 Hz (range of approximately 10 to 30 Hz), determined based on known GCaMP6s kinetics (Chen et al. 2013).

Five mice were used in the BF-ACh study. Across 15 sessions, 397 axon segments were imaged. In the LC-NA study, 6 mice were used. Across 18 sessions, 283 axon segments were imaged. Seven mice were used for the VCIN study. Across 12 sessions, 98 cell bodies were imaged. Recording duration varied between ~10 min and 40 min.

Statistical Analysis

Behavioral Data Analysis

All imaging data was first aligned to behavioral data using custom Matlab scripts. Pupil diameter was normalized to the max pupil diameter in each session to limit overestimation of arousal state in low lighting conditions. FaceMap (https://github.com/MouseLand/FaceMap) was used to calculate motion energy of the snout and mouth. Onsets and offsets of walking bouts, whisking bouts, and facial twitches were detected using custom Matlab code. Walking bouts were defined as times during which the mouse exceeded a speed of 2.5 cm/s for at least 2 seconds. Whisker pad motion energy was normalized between 0 and 1 for each session and

whisking bouts were defined as periods in which the normalized whisker pad motion energy exceeded 20% for more than 1 s. Twitches were defined as moments when the normalized whisker pad motion energy exceeded 20% for less than 0.5 s. Walking bouts, whisking bouts, and twitches that were not preceded and followed by 1 s of stillness were excluded. For the BF-ACh study, GCaMP6s activity in 397 axon segments was compared to 101 waking onsets and offsets, 330 whisking onsets, 201 whisking offsets, and 1108 twitch onsets. For the LC-NA study, GCaMP6s activity in 283 axon segments was compared to 34 walking onsets and offsets, 400 whisk onsets, 353 whisk offsets, and 644 twitch onsets. For the VCIN study GCaMP6s activity in 84 cell bodies was compared to 127 walking onsets and offsets and activity in 98 cell bodies was compared to 1104 whisking onsets, 1015 whisking offsets, and 870 twitch onsets.

2-Photon Imaging Analysis

Suite2P (Pachitariu et al., 2017) was used to identify cells and axons from 2-photon mesoscope imaging data. All identified cells and axons were manually verified and any identified regions that did not correspond to a clearly identifiable distinct cell or axon were excluded. Axons and cell body regions that were identified with Suite2P but were visually confirmed (i.e. clear continuity of axon form, within the imaging plane, connecting the two segments together) to belong to the same cell or axon were removed from our experimental data set and included in our same-axon/cell data set (ACh: n = 18; NA: n = 30; VCIN: n = 18). To control for the possibility of motion artifacts, autofluorescent “blebs” that did not have calcium-dependent activity, and were approximately of similar size to axonal varicosities, were selected from within the imaging fields (ACh: n = 22; NA: n = 19; VCIN: n = 8). Distances between ROIs (Fig. 1, 4, 5) were determined based on the center point of each ROI. ROI size ranged from 50x50 to 400x400 µm.

Pre-processing of calcium fluorescence data was performed using methods previously described (Reimer et al. 2016; Nelson and Mooney 2016b). Briefly, all traces were upsampled to 100 Hz and lowpass filtered to 10 Hz. Signal-to-noise ratios were then calculated for all traces by dividing the max power between the frequency range of 0.05-0.5 Hz by the mean power between 1-3 Hz. All traces that did not meet a minimum signal-to-noise criteria of log(20) were excluded from further analyses. Normalized fluorescence values were used in statistical analyses to avoid over-weighting larger or brighter axon segments. For displaying data, $\Delta F/F$ was calculated using the median fluorescence value over each recording session as the baseline fluorescence. All preprocessing was performed using custom Matlab scripts.

Relationships between behavior and axon activity

To determine the frequencies at which axonal GCaMP6s fluorescence and arousal-related behaviors (walking, pupil dilation, facial movement) were most correlated, magnitude-squared coherence was calculated using a 2 min window with a 98% overlap and a Hamming filter using the Matlab function mscohere. As a control, axon activity traces were shuffled in time and coherence was calculated with all behavioral variables.

To assess the timing of axonal activity (GCaMP6s fluorescence) in comparison to arousal-related behaviors, cross correlations between axon activity and behavioral measures

were calculated using the Matlab function xcorr with a 3 s maximum lag. Cross correlations were calculated after low pass filtering at 1 Hz to capture the frequencies at which our behavioral variables and GCaMP6s have the most power (Fig. S3).

Ridge regressions were used to determine the relative strength of the relationships between behavioral variables and axon activity. All data was first low pass filtered at 1 Hz. Models were cross validated to account for overfitting.

Relationships between axons/cells

Magnitude-squared coherence and cross-correlation was calculated between all pairs of simultaneously recorded axons using the same parameters used to relate axon activity to behavior, as described above. Distance between axons was estimated by calculating the distance between the center point of each ROI. Therefore, axons within the same ROI were coded as 0 mm apart.

But first, since our data may be strongly influenced by the frequency of activity occurring in the axons (owing to the preference of GCaMP6s fluorescence for low frequencies: Fig. S3), we sought to better understand the limitations of our activity monitoring methodology by comparing the coherence and correlation of activity in two adjacent segments of the same axon (Figs. 4, S3). Since axon conduction failures are rare (Foust et al. 2010; Popovic et al. 2011), we reasoned that any decrease below 100% coherence or below a correlation of 1 would indicate a fundamental limitation of the data. This limitation results from the complex relationship between axonal action potential activity, $[Ca^{2+}]_i$, GCaMP6s, and our ability to monitor axonal GCaMP6s fluorescence.

To this end, first we identified several (n = 18 ACh; n = 30 NA) pairs of adjacent axon segments that we determined by eye to be portions of the same axon (i.e. segments joined by a clear continuity of axonal form). Comparison of the signal in these two adjacent segments of the same cholinergic or noradrenergic axon revealed strong signal at low frequencies (< 1 Hz), but also strong variations in signal at frequencies greater than approximately 1 Hz (Fig. 4D-E). Plots of coherence between adjacent segments of the same axon revealed high (e.g. >/= 0.8) values at frequencies below approximately 1 Hz, but this coherence decreased strongly at frequencies above approximately 1 Hz, such that the coherence between the axon segments was similar to that obtained with shuffled data at frequencies > approximately 3 Hz (Fig. 4D,E). This result indicates that our measure of axonal activity is limited to variations in action potential firing rate below approximately 1 Hz. Therefore, we applied a 1 Hz low pass filter to the recordings prior to calculation of correlation. Examining different cut off frequencies for the low pass filter indicated that a cutoff frequency of 1 Hz was optimal for enhancing correlation in same-axon data, while preserving information (see Fig. S5A,B).

Since we observed a broad distribution in cross correlation between simultaneously recorded axons or cells (Fig. 4 F-G), we used a partial correlation analysis to determine whether some pairs were highly correlated due to a shared “common signal”. Partial correlations were calculated by correlating the residuals of a linear regression between a controlling variable, or

common signal, (described below) and each of two axons or cells in a pair using the Matlab function partialcorr. The average dF/F of all simultaneously recorded axons or cells (excluding the two axons or cells being compared) was used as a controlling variable. Counts of simultaneously imaged axons or cells ranged from 7-61 for ACh, 9-24 for NA, and 3-10 for VCINs. Since our data suggest that facial activity could contribute to the common signal, we also used whisking activity as the controlling variable in a separate analysis (Fig. S5 E,F). Partial correlations were calculated after low pass filtering at 1 Hz. To determine the impact of behavioral state on partial correlation, periods in which the animal was stationary (not walking) and still (neither walking nor whisking) were isolated.

Custom Matlab scripts used in data analysis are available online at www.github.com/lncollins91/ACh_NA_VCIN.

References

Aston-Jones, Gary, and Jonathan D. Cohen. 2005. "An Integrative Theory of Locus Coeruleus-Norepinephrine Function: Adaptive Gain and Optimal Performance." *Annual Review of Neuroscience* 28: 403–50.

Aston-Jones, G., and F. E. Bloom. 1981. "Activity of Norepinephrine-Containing Locus Coeruleus Neurons in Behaving Rats Anticipates Fluctuations in the Sleep-Waking Cycle." *The Journal of Neuroscience*. https://doi.org/10.1523/jneurosci.01-08-00876.1981.

Berridge, Craig W. 2008. "Noradrenergic Modulation of Arousal." *Brain Research Reviews* 58 (1): 1–17.

Breton-Provencher, Vincent, Gabrielle T. Drummond, Jiesi Feng, Yulong Li, and Mriganka Sur. 2022. "Spatiotemporal Dynamics of Noradrenaline during Learned Behaviour." *Nature*, June. https://doi.org/10.1038/s41586-022-04782-2.

Breton-Provencher, Vincent, and Mriganka Sur. 2019. "Active Control of Arousal by a Locus Coeruleus GABAergic Circuit." *Nature Neuroscience* 22 (2): 218–28.

Buzsaki, G., R. G. Bickford, G. Ponomareff, L. J. Thal, R. Mandel, and F. H. Gage. 1988. "Nucleus Basalis and Thalamic Control of Neocortical Activity in the Freely Moving Rat." *The Journal of Neuroscience: The Official Journal of the Society for Neuroscience* 8 (11): 4007–26.

Carter, Matthew E., Ofer Yizhar, Sachiko Chikahisa, Hieu Nguyen, Antoine Adamantidis, Seiji Nishino, Karl Deisseroth, and Luis de Lecea. 2010. "Tuning Arousal with Optogenetic Modulation of Locus Coeruleus Neurons." *Nature Neuroscience* 13 (12): 1526–33.

Chandler, Daniel J., Wen-Jun Gao, and Barry D. Waterhouse. 2014. "Heterogeneous Organization of the Locus Coeruleus Projections to Prefrontal and Motor Cortices." *Proceedings of the National Academy of Sciences*. https://doi.org/10.1073/pnas.1320827111.

Chandler, Daniel, and Barry D. Waterhouse. 2012. "Evidence for Broad versus Segregated Projections from Cholinergic and Noradrenergic Nuclei to Functionally and Anatomically Discrete Subregions of Prefrontal Cortex." *Frontiers in Behavioral Neuroscience* 6 (May): 20.

Chandler, Dan J., Patricia Jensen, Jordan G. McCall, Anthony E. Pickering, Lindsay A. Schwarz, and Nelson K. Totah. 2019. "Redefining Noradrenergic Neuromodulation of Behavior: Impacts of a Modular Locus Coeruleus Architecture." *The Journal of Neuroscience: The Official Journal of the Society for Neuroscience* 39 (42): 8239–49.

Chen, Tsai-Wen, Trevor J. Wardill, Yi Sun, Stefan R. Pulver, Sabine L. Renninger, Amy Baohan, Eric R. Schreiter, et al. 2013. "Ultrasensitive Fluorescent Proteins for Imaging Neuronal Activity." *Nature*.

https://doi.org/10.1038/nature12354.
Dasgupta, Rajan, Frederik Seibt, and Michael Beierlein. 2018. “Synaptic Release of Acetylcholine Rapidly Suppresses Cortical Activity by Recruiting Muscarinic Receptors in Layer 4.” *The Journal of Neuroscience: The Official Journal of the Society for Neuroscience* 38 (23): 5338–50.
Deitcher, Yair, Yonatan Leibner, Sara Kutzkel, Neta Zylbermann, and Michael London. 2019. “Nonlinear Relationship between Multimodal Adrenergic Responses and Local Dendritic Activity in Primary Sensory Cortices.” *bioRxiv.* https://doi.org/10.1101/814657.
Dipoppa, Mario, Adam Ranson, Michael Krumin, Marius Pachitariu, Matteo Carandini, and Kenneth D. Harris. 2018. “Vision and Locomotion Shape the Interactions between Neuron Types in Mouse Visual Cortex.” *Neuron* 98 (3): 602–15.e8.
Dudai, Amir, Nadav Yayon, Hermona Soreq, and Michael London. 2021. “Cortical VIP /ChAT Interneurons: From Genetics to Function.” *Journal of Neurochemistry*. https://doi.org/10.1111/jnc.15263.
Eggermann, Emmanuel, Yves Kremer, Sylvain Crochet, and Carl C. H. Petersen. 2014. “Cholinergic Signals in Mouse Barrel Cortex during Active Whisker Sensing.” *Cell Reports* 9 (5): 1654–60.
Ego-Stengel, Valérie, Daniel E. Shulz, Sebastian Haidarliu, Ronen Sosnik, and Ehud Ahissar. 2001. “Acetylcholine-Dependent Induction and Expression of Functional Plasticity in the Barrel Cortex of the Adult Rat.” *Journal of Neurophysiology*. https://doi.org/10.1152/jn.2001.86.1.422.
Flavell, Steven W., Nadine Gogolla, Matthew Lovett-Barron, and Moriel Zelikowsky. 2022. “The Emergence and Influence of Internal States.” *Neuron*, May. https://doi.org/10.1016/j.neuron.2022.04.030.
Foust, Amanda, Marko Popovic, Dejan Zecevic, and David A. McCormick. 2010. “Action Potentials Initiate in the Axon Initial Segment and Propagate through Axon Collaterals Reliably in Cerebellar Purkinje Neurons.” *The Journal of Neuroscience: The Official Journal of the Society for Neuroscience* 30 (20): 6891–6902.
Fu, Yu, Jason M. Tucciarone, J. Sebastian Espinosa, Nengyin Sheng, Daniel P. Darcy, Roger A. Nicoll, Z. Josh Huang, and Michael P. Stryker. 2014. “A Cortical Circuit for Gain Control by Behavioral State.” *Cell* 156 (6): 1139–52.
Gielow, Matthew R., and Laszlo Zaborszky. 2017. “The Input-Output Relationship of the Cholinergic Basal Forebrain.” *Cell Reports*. https://doi.org/10.1016/j.celrep.2017.01.060.
Giustino, Thomas F., and Stephen Maren. 2018. “Noradrenergic Modulation of Fear Conditioning and Extinction.” *Frontiers in Behavioral Neuroscience* 12 (March): 43.
Goard, Michael, and Yang Dan. 2009. “Basal Forebrain Activation Enhances Cortical Coding of Natural Scenes.” *Nature Neuroscience* 12 (11): 1444–49.
Granger, Adam J., Wengang Wang, Keiramarie Robertson, Mahmoud El-Rifai, Andrea F. Zanello, Karina Bistrong, Arpiar Saunders, et al. 2020. “Cortical ChAT+ Neurons Co-Transmit Acetylcholine and GABA in a Target- and Brain-Region-Specific Manner.” *eLife* 9 (July). https://doi.org/10.7554/eLife.57749.
Han, Yong, Yu-Feng Shi, Wang Xi, Rui Zhou, Zhi-Bing Tan, Hao Wang, Xiao-Ming Li, et al. 2014. “Selective Activation of Cholinergic Basal Forebrain Neurons Induces Immediate Sleep-Wake Transitions.” *Current Biology: CB* 24 (6): 693–98.
Harris, Kenneth D. 2021. “Nonsense Correlations in Neuroscience.” *bioRxiv.* https://doi.org/10.1101/2020.11.29.402719.
Harrison, Thomas C., Lucas Pinto, Julien R. Brock, and Yang Dan. 2016. “Calcium Imaging of Basal Forebrain Activity during Innate and Learned Behaviors.” *Frontiers in Neural Circuits* 10 (May): 36.
Hedrick, Tristan, and Jack Waters. 2015. “Acetylcholine Excites Neocortical Pyramidal Neurons via Nicotinic Receptors.” *Journal of Neurophysiology*. https://doi.org/10.1152/jn.00716.2014.
Hobson, J. Allan, J. Allan Hobson, Robert W. McCarley, and Peter W. Wyzinski. 1975. “Sleep Cycle

Oscillation: Reciprocal Discharge by Two Brainstem Neuronal Groups." *Science*. https://doi.org/10.1126/science.1094539.

Howe, Mark, Imane Ridouh, Anna Letizia Allegra Mascaro, Alyssa Larios, Maite Azcorra, and Daniel A. Dombeck. 2019. "Coordination of Rapid Cholinergic and Dopaminergic Signaling in Striatum during Spontaneous Movement." *eLife* 8 (March). https://doi.org/10.7554/eLife.44903.

Huppé-Gourgues, Frédéric, Karim Jegouic, and Elvire Vaucher. 2018. "Topographic Organization of Cholinergic Innervation From the Basal Forebrain to the Visual Cortex in the Rat." *Frontiers in Neural Circuits* 12 (March): 19.

Irmak, Simal Ozen, and Luis de Lecea. 2014. "Basal Forebrain Cholinergic Modulation of Sleep Transitions." *Sleep* 37 (12): 1941–51.

Janitzky, Kathrin, Michael T. Lippert, Achim Engelhorn, Jennifer Tegtmeier, Jürgen Goldschmidt, Hans-Jochen Heinze, and Frank W. Ohl. 2015. "Optogenetic Silencing of Locus Coeruleus Activity in Mice Impairs Cognitive Flexibility in an Attentional Set-Shifting Task." *Frontiers in Behavioral Neuroscience* 9 (November): 286.

Joshi, Siddhartha, and Joshua I. Gold. 2022. "Context-Dependent Relationships between Locus Coeruleus Firing Patterns and Coordinated Neural Activity in the Anterior Cingulate Cortex." *eLife* 11 (January). https://doi.org/10.7554/eLife.63490.

Joshi, Siddhartha, Yin Li, Rishi M. Kalwani, and Joshua I. Gold. 2016. "Relationships between Pupil Diameter and Neuronal Activity in the Locus Coeruleus, Colliculi, and Cingulate Cortex." *Neuron* 89 (1): 221–34.

Kim, Jae-Hyun, A-Hyun Jung, Daun Jeong, Ilsong Choi, Kwansoo Kim, Soowon Shin, Sung June Kim, and Seung-Hee Lee. 2016. "Selectivity of Neuromodulatory Projections from the Basal Forebrain and Locus Ceruleus to Primary Sensory Cortices." *The Journal of Neuroscience: The Official Journal of the Society for Neuroscience* 36 (19): 5314–27.

Larsen, Rylan S., and Jack Waters. 2018. "Neuromodulatory Correlates of Pupil Dilation." *Frontiers in Neural Circuits* 12 (March): 21.

Lee, Maan Gee, Oum K. Hassani, Angel Alonso, and Barbara E. Jones. 2005. "Cholinergic Basal Forebrain Neurons Burst with Theta during Waking and Paradoxical Sleep." *Journal of Neuroscience* 25 (17): 4365–69.

Lee, Seung-Hee, and Yang Dan. 2012. "Neuromodulation of Brain States." *Neuron*. https://doi.org/10.1016/j.neuron.2012.09.012.

Lohani, Sweyta, Andrew H. Moberly, Hadas Benisty, Boris Landa, Miao Jing, Yulong Li, Michael J. Higley, and Jessica A. Cardin. 2021. "Dual Color Mesoscopic Imaging Reveals Spatiotemporally Heterogeneous Coordination of Cholinergic and Neocortical Activity." *bioRxiv*. https://doi.org/10.1101/2020.12.09.418632.

Loughlin, S. E., S. L. Foote, and F. E. Bloom. 1986. "Efferent Projections of Nucleus Locus Coeruleus: Topographic Organization of Cells of Origin Demonstrated by Three-Dimensional Reconstruction." *Neuroscience* 18 (2): 291–306.

Loughlin, S. E., S. L. Foote, and J. H. Fallon. 1982. "Locus Coeruleus Projections to Cortex: Topography, Morphology and Collateralization." *Brain Research Bulletin* 9 (1-6): 287–94.

McCormick, D. A. 1989. "Cholinergic and Noradrenergic Modulation of Thalamocortical Processing." *Trends in Neurosciences* 12 (6): 215–21.

McCormick, D.A. 1992. "Neurotransmitter Actions in the Thalamus and Cerebral Cortex and Their Role in Neuromodulation of Thalamocortical Activity." *Progress in Neurobiology* 39 (4): 337–88.

McCormick, David A., Dennis B. Nestvogel, and Biyu J. He. 2020. "Neuromodulation of Brain State and Behavior." *Annual Review of Neuroscience* 43 (July): 391–415.

McGinley, Matthew J., Stephen V. David, and David A. McCormick. 2015. "Cortical Membrane Potential Signature of Optimal States for Sensory Signal Detection." *Neuron* 87 (1): 179–92.

McGinley, Matthew J., Martin Vinck, Jacob Reimer, Renata Batista-Brito, Edward Zagha, Cathryn R. Cadwell, Andreas S. Tolias, Jessica A. Cardin, and David A. McCormick. 2015. "Waking State: Rapid Variations Modulate Neural and Behavioral Responses." *Neuron* 87 (6): 1143–61.

Mechawar, N., C. Cozzari, and L. Descarries. 2000. "Cholinergic Innervation in Adult Rat Cerebral Cortex: A Quantitative Immunocytochemical Description." *The Journal of Comparative Neurology* 428 (2): 305–18.

Megemont, Marine, Jim McBurney-Lin, and Hongdian Yang. 2022. "Pupil Diameter Is Not an Accurate Real-Time Readout of Locus Coeruleus Activity." *eLife* 11 (February). https://doi.org/10.7554/eLife.70510.

Metherate, R., and J. H. Ashe. 1993. "Nucleus Basalis Stimulation Facilitates Thalamocortical Synaptic Transmission in the Rat Auditory Cortex." *Synapse* 14 (2): 132–43.

Metherate, R., C. L. Cox, and J. H. Ashe. 1992. "Cellular Bases of Neocortical Activation: Modulation of Neural Oscillations by the Nucleus Basalis and Endogenous Acetylcholine." *The Journal of Neuroscience*. https://doi.org/10.1523/jneurosci.12-12-04701.1992.

Mobley, P., and P. Greengard. 1985. "Evidence for Widespread Effects of Noradrenaline on Axon Terminals in the Rat Frontal Cortex." *Proceedings of the National Academy of Sciences of the United States of America* 82 (3): 945–47.

Muñoz, William, Robin Tremblay, Daniel Levenstein, and Bernardo Rudy. 2017. "Layer-Specific Modulation of Neocortical Dendritic Inhibition during Active Wakefulness." *Science* 355 (6328): 954–59.

Musall, Simon, Matthew T. Kaufman, Ashley L. Juavinett, Steven Gluf, and Anne K. Churchland. 2019. "Single-Trial Neural Dynamics Are Dominated by Richly Varied Movements." *Nature Neuroscience* 22 (10): 1677–86.

Nelson, Anders, and Richard Mooney. 2016a. "The Basal Forebrain and Motor Cortex Provide Convergent yet Distinct Movement-Related Inputs to the Auditory Cortex." *Neuron*. https://doi.org/10.1016/j.neuron.2016.03.031.

Nestvogel, Dennis B., and David A. McCormick. 2022. "Visual Thalamocortical Mechanisms of Waking State-Dependent Activity and Alpha Oscillations." *Neuron* 110 (1): 120–38.e4.

Niell, Cristopher M., and Michael P. Stryker. 2010. "Modulation of Visual Responses by Behavioral State in Mouse Visual Cortex." *Neuron* 65 (4): 472–79.

Noei, Shahryar, Ioannis S. Zouridis, Nikos K. Logothetis, Stefano Panzeri, and Nelson K. Totah. 2022. "Distinct Ensembles in the Noradrenergic Locus Coeruleus Are Associated with Diverse Cortical States." *Proceedings of the National Academy of Sciences* 119 (18): e2116507119.

Obermayer, Joshua, Antonio Luchicchi, Tim S. Heistek, Sybren F. de Kloet, Huub Terra, Bastiaan Bruinsma, Ouissame Mnie-Filali, et al. 2019. "Prefrontal Cortical ChAT-VIP Interneurons Provide Local Excitation by Cholinergic Synaptic Transmission and Control Attention." *Nature Communications* 10 (1): 5280.

Pachitariu, Marius, Carsen Stringer, Mario Dipoppa, Sylvia Schröder, L. Federico Rossi, Henry Dalgleish, Matteo Carandini, and Kenneth D. Harris. 2017. "Suite2p: Beyond 10,000 Neurons with Standard Two-Photon Microscopy." *bioRxiv.* https://doi.org/10.1101/061507.

Petersen, Carl C. H. 2019. "Sensorimotor Processing in the Rodent Barrel Cortex." *Nature Reviews. Neuroscience* 20 (9): 533–46.

Picciotto, Marina R., Michael J. Higley, and Yann S. Mineur. 2012. "Acetylcholine as a Neuromodulator: Cholinergic Signaling Shapes Nervous System Function and Behavior." *Neuron* 76 (1): 116–29.

Pinto, Lucas, Michael J. Goard, Daniel Estandian, Min Xu, Alex C. Kwan, Seung-Hee Lee, Thomas C. Harrison, Guoping Feng, and Yang Dan. 2013. "Fast Modulation of Visual Perception by Basal Forebrain Cholinergic Neurons." *Nature Neuroscience* 16 (12): 1857–63.

Poe, Gina R., Stephen Foote, Oxana Eschenko, Joshua P. Johansen, Sebastien Bouret, Gary Aston-Jones,

Carolyn W. Harley, et al. 2020. “Locus Coeruleus: A New Look at the Blue Spot.” *Nature Reviews Neuroscience*. https://doi.org/10.1038/s41583-020-0360-9.

Polack, Pierre-Olivier, Jonathan Friedman, and Peyman Golshani. 2013. “Cellular Mechanisms of Brain State-Dependent Gain Modulation in Visual Cortex.” *Nature Neuroscience* 16 (9): 1331–39.

Popovic, Marko A., Amanda J. Foust, David A. McCormick, and Dejan Zecevic. 2011. “The Spatio-Temporal Characteristics of Action Potential Initiation in Layer 5 Pyramidal Neurons: A Voltage Imaging Study.” *The Journal of Physiology* 589 (17): 4167–87.

Poulet, James F. A., and Sylvain Crochet. 2018. “The Cortical States of Wakefulness.” *Frontiers in Systems Neuroscience* 12: 64.

Reimer, Jacob, Emmanouil Froudarakis, Cathryn R. Cadwell, Dimitri Yatsenko, George H. Denfield, and Andreas S. Tolias. 2014. “Pupil Fluctuations Track Fast Switching of Cortical States during Quiet Wakefulness.” *Neuron* 84 (2): 355–62.

Reimer, Jacob, Matthew J. McGinley, Yang Liu, Charles Rodenkirch, Qi Wang, David A. McCormick, and Andreas S. Tolias. 2016. “Pupil Fluctuations Track Rapid Changes in Adrenergic and Cholinergic Activity in Cortex.” *Nature Communications* 7 (November): 13289.

Robert, Blaise, Eyal Y. Kimchi, Yurika Watanabe, Tatenda Chakoma, Miao Jing, Yulong Li, and Daniel B. Polley. 2021. “A Functional Topography within the Cholinergic Basal Forebrain for Encoding Sensory Cues and Behavioral Reinforcement Outcomes.” *eLife* 10 (November). https://doi.org/10.7554/eLife.69514.

Sachidhanandam, Shankar, Varun Sreenivasan, Alexandros Kyriakatos, Yves Kremer, and Carl C. H. Petersen. 2013. “Membrane Potential Correlates of Sensory Perception in Mouse Barrel Cortex.” *Nature Neuroscience* 16 (11): 1671–77.

Salkoff, David B., Edward Zagha, Erin McCarthy, and David A. McCormick. 2020. “Movement and Performance Explain Widespread Cortical Activity in a Visual Detection Task.” *Cerebral Cortex*. https://doi.org/10.1093/cercor/bhz206.

Sara, Susan J. 2009. “The Locus Coeruleus and Noradrenergic Modulation of Cognition.” *Nature Reviews. Neuroscience* 10 (3): 211–23.

Sara, Susan J., and Sebastien Bouret. 2012. “Orienting and Reorienting: The Locus Coeruleus Mediates Cognition through Arousal.” *Neuron* 76 (1): 130–41.

Schwarz, Lindsay A., and Liqun Luo. 2015. “Organization of the Locus Coeruleus-Norepinephrine System.” *Current Biology: CB* 25 (21): R1051–56.

Schwarz, Lindsay A., Kazunari Miyamichi, Xiaojing J. Gao, Kevin T. Beier, Brandon Weissbourd, Katherine E. DeLoach, Jing Ren, et al. 2015. “Viral-Genetic Tracing of the Input–output Organization of a Central Noradrenaline Circuit.” *Nature*. https://doi.org/10.1038/nature14600.

Sofroniew, Nicholas James, Daniel Flickinger, Jonathan King, and Karel Svoboda. 2016. “A Large Field of View Two-Photon Mesoscope with Subcellular Resolution for in Vivo Imaging.” *eLife* 5 (June). https://doi.org/10.7554/eLife.14472.

Steinmetz, Nicholas A., Peter Zatka-Haas, Matteo Carandini, and Kenneth D. Harris. 2019. “Distributed Coding of Choice, Action and Engagement across the Mouse Brain.” *Nature* 576 (7786): 266–73.

Stringer, Carsen, Marius Pachitariu, Nicholas Steinmetz, Charu Bai Reddy, Matteo Carandini, and Kenneth D. Harris. 2019. “Spontaneous Behaviors Drive Multidimensional, Brainwide Activity.” *Science* 364 (6437): 255.

Sturgill, J. F., P. Hegedus, S. J. Li, Q. Chevy, A. Siebels, M. Jing, Y. Li, B. Hangya, and A. Kepecs. 2020. “Basal Forebrain-Derived Acetylcholine Encodes Valence-Free Reinforcement Prediction Error.” *bioRxiv*. https://doi.org/10.1101/2020.02.17.953141.

Teles-Grilo Ruivo, Leonor M., Keeley L. Baker, Michael W. Conway, Peter J. Kinsley, Gary Gilmour, Keith G. Phillips, John T. R. Isaac, John P. Lowry, and Jack R. Mellor. 2017. “Coordinated Acetylcholine Release in Prefrontal Cortex and Hippocampus Is Associated with Arousal and Reward on Distinct

Timescales." *Cell Reports* 18 (4): 905–17.
Totah, Nelson K. B., Nikos K. Logothetis, and Oxana Eschenko. 2019. "Noradrenergic Ensemble-Based Modulation of Cognition over Multiple Timescales." *Brain Research* 1709 (April): 50–66.
Totah, Nelson K., Ricardo M. Neves, Stefano Panzeri, Nikos K. Logothetis, and Oxana Eschenko. 2018. "The Locus Coeruleus Is a Complex and Differentiated Neuromodulatory System." *Neuron* 99 (5): 1055–68.e6.
Uematsu, Akira, Bao Zhen Tan, Edgar A. Ycu, Jessica Sulkes Cuevas, Jenny Koivumaa, Felix Junyent, Eric J. Kremer, Ilana B. Witten, Karl Deisseroth, and Joshua P. Johansen. 2017. "Modular Organization of the Brainstem Noradrenaline System Coordinates Opposing Learning States." *Nature Neuroscience* 20 (11): 1602–11.
Usher, M. 1999. "The Role of Locus Coeruleus in the Regulation of Cognitive Performance." *Science*. https://doi.org/10.1126/science.283.5401.549.
Vinck, Martin, Renata Batista-Brito, Ulf Knoblich, and Jessica A. Cardin. 2015. "Arousal and Locomotion Make Distinct Contributions to Cortical Activity Patterns and Visual Encoding." *Neuron* 86 (3): 740–54.
Wang, Quanxin, Song-Lin Ding, Yang Li, Josh Royall, David Feng, Phil Lesnar, Nile Graddis, et al. 2020. "The Allen Mouse Brain Common Coordinate Framework: A 3D Reference Atlas." *Cell* 181 (4): 936–53.e20.
Waterhouse, B. D., C. S. Lin, R. A. Burne, and D. J. Woodward. 1983. "The Distribution of Neocortical Projection Neurons in the Locus Coeruleus." *The Journal of Comparative Neurology* 217 (4): 418–31.
Williams, J. A., J. Comisarow, J. Day, H. C. Fibiger, and P. B. Reiner. 1994. "State-Dependent Release of Acetylcholine in Rat Thalamus Measured by in Vivo Microdialysis." *The Journal of Neuroscience: The Official Journal of the Society for Neuroscience* 14 (9): 5236–42.
Xu, Min, Shinjae Chung, Siyu Zhang, Peng Zhong, Chenyan Ma, Wei-Cheng Chang, Brandon Weissbourd, et al. 2015. "Basal Forebrain Circuit for Sleep-Wake Control." *Nature Neuroscience* 18 (11): 1641–47.
Yu, Jianing, Hang Hu, Ariel Agmon, and Karel Svoboda. 2019. "Recruitment of GABAergic Interneurons in the Barrel Cortex during Active Tactile Behavior." *Neuron* 104 (2): 412–27.e4.
Zaborszky, Laszlo, Attila Csordas, Kevin Mosca, Joseph Kim, Matthew R. Gielow, Csaba Vadasz, and Zoltan Nadasdy. 2015. "Neurons in the Basal Forebrain Project to the Cortex in a Complex Topographic Organization That Reflects Corticocortical Connectivity Patterns: An Experimental Study Based on Retrograde Tracing and 3D Reconstruction." *Cerebral Cortex*. https://doi.org/10.1093/cercor/bht210.
Zant, Janneke C., Tae Kim, Laszlo Prokai, Szabolcs Szarka, James McNally, James T. McKenna, Charu Shukla, et al. 2016. "Cholinergic Neurons in the Basal Forebrain Promote Wakefulness by Actions on Neighboring Non-Cholinergic Neurons: An Opto-Dialysis Study." *The Journal of Neuroscience: The Official Journal of the Society for Neuroscience* 36 (6): 2057–67.